Climatic and environmental change in the western Tibetan Plateau during the Holocene, recorded by lake sediments from Aweng Co

Yuzhi Zhang [a], Jiawu Zhang [a, *], Suzanne McGowan [b], Sarah Metcalfe [b],

Matthew Jones [b,c], Melanie J. Leng [d,e], Juzhi Hou [f]

[a] Key Laboratory of Western China's Environmental Systems (Ministry of Education), College of Earth and Environmental Sciences, Lanzhou University, Lanzhou, 730000, China

[b] School of Geography, University of Nottingham, Nottingham, NG7 2RD, UK

[c] Future Food Beacon, University of Nottingham, Nottingham, NG7 2RG, UK

[d] National Environmental Isotope Facility, British Geological Survey, Nottingham, NG12 5GG, UK

[e] Centre for Environmental Geochemistry, School of Biosciences, University of Nottingham, Loughborough, LE12 5RD, UK

[f] Key Laboratory of Tibetan Environment Changes and Land Surface Processes, Institute of Tibetan Plateau Research, Chinese Academy of Sciences, Beijing, 100101, China

* Corresponding author.

E-mail address: jwzhang@lzu.edu.cn

Abstract: Understanding the strength and extent of the Asian summer monsoon (including the East Asian summer monsoon and the Indian summer monsoon) in the Tibetan Plateau (TP) region is crucial for predicting possible changes in the regional eco-environment and water resources under global warming. Due to the lack of well-dated and high-resolution paleoclimate records, long-term monsoon dynamics are still not well understood in the western TP, which is currently influenced by both the Indian summer monsoon (ISM) and the westerlies. Here we present a multi-proxy lacustrine record covering the past 10,500 years from Aweng Co, an alpine lake at the northern limit of the modern ASM in western Tibet. Our results show that the western TP was mainly controlled by the ISM during the Holocene and the regional ecosystem/environment was sensitive to climate change. The climate was the wettest between 10.5-7.3 cal. kyr BP, when terrestrial plants in the catchment were productive and the biomass of benthic algae was low possibly due to limited sunlight at the lake bottom due to high lake level. From 7.3 to 5.0 cal. kyr BP the climate shifted towards drier conditions, resulting in a decline in terrestrial plant cover. Between 5.0 and 3.1 cal. kyr BP, the climate became even drier, resulting in a further decline in vegetation cover in the catchment. Between 4.6 and 3.1 cal. kyr BP, 100% endogenic dolomite precipitated from the lake water, possibly induced by high Mg/Ca ratios. After 3.1 cal. kyr BP, the climate was the driest and frequent centennial-scale droughts occurred. The lake level was low and would have resulted in more light reaching the lake bottom, favoring the growth of benthic algae. The reconstructed lake level change of Aweng Co agrees well with the paleo-shoreline records in the southern TP, demonstrating that the ISM evolution played a key role in lake hydrological processes in this region. A comparison of paleoclimate records shows the ISM reached 34.5° N in the western TP during the Holocene.

Key words: Indian summer monsoon, paleoclimate, lake level, stable isotopes, ostracods

1 Introduction

Climate change in the Tibetan Plateau (TP) is important because it influences both the vulnerable ecological environment at high elevations and the water supply for 85% of the Asian population (Huang et al., 2008). Currently, the Asian summer monsoon (ASM), including the East Asian summer monsoon (EASM) and the Indian summer monsoon (ISM), carries moisture to around 30° N in the TP region, as suggested by records of oxygen isotopes in precipitation ($\delta^{18}O_p$) and atmospheric model simulations (Tian et al., 2007; Yao et al., 2013). Climate in the area to the north of 35° N is dominated by the westerlies (Tian et al., 2007; Yao et al., 2013). Therefore, between 30° N and 35° N in the TP, precipitation is either from the ASM, or the westerlies, or both, depending on the strength of the respective climate systems. Variability in the northern limit (or the maximum extent) of the ASM over the Holocene is not well defined, although it is linked to shifts in the position of the Intertropical Convergence Zone (ITCZ) (Clement et al., 1996; Clement, 1999). Numerous paleoclimate studies have looked at the northern extent of the ASM during the Holocene in the northeastern TP, such as those from Qinghai Lake (Henderson et al., 2010, An et al., 2012), Herleg Lake (Zhao et al., 2013) and Genggahai Lake (Qiang et al., 2017). In the western TP, however, relatively few studies have been carried out for similar purposes (Hou et al., 2017; Li et al., 2017a).

Although some studies were carried out in the western TP during the 1990s e.g. at Bangong Co (Gasse et al., 1996; Fan et al., 1996), Longmu Co (Avouac et al., 1996) and Sumxi Co (Gasse et al., 1991), the resolution of these lake sediment sequences was generally low, and unsuitable for making detailed comparisons with high-resolution records. More paleoclimate records, especially from the western TP, are therefore required to understand the variability in the ASM, and the related environmental history.

Here we present a lacustrine record of climatic and environmental change during the Holocene from Aweng Co, an alpine lake at the modern ASM boundary in the western TP, with the aim of reconstructing a reliable climate history and the terrestrial and aquatic ecological environmental history during the Holocene. Geochemical proxies (stable isotopes of endogenic carbonates and ostracod shells) are used to reconstruct the paleoclimate, and bio-geochemical proxies (total organic content, C/N ratios and carbon isotope of organic matter $\delta^{13}C_{org}$) are used to reconstruct the responses of the terrestrial-aquatic ecosystems to climate change during the Holocene. Reliable records in the southern and western TP are then compared to investigate the regional climate and the northern limit of the ISM in the western TP during the Holocene.

2 Study Site

Aweng Co (32.7°–32.81° N, 81.63°–81.8° E; Fig. 1A) is a closed saline lake located in the western TP. The altitude of the lake is 4,430 m a.s.l. and the surrounding hills are 500 m higher (Wang and Dou, 1998). The catchment mainly consists of Cretaceous granite and Jurassic metamorphosed sandstone (Zhou et al., 2011). The main vegetation in the catchment is alpine desert steppe, dominated by C_3 *Stipa* spp grasses. Aweng Co is 23.4 km long with a mean and maximum width of 2.52 km and 5.3 km, respectively. In 2015, the maximum water depth was 6 m and the lake area was 68.96 km^2. There are clear paleo-shorelines around the southeastern part of the lake, indicating that the lake level was once much higher than at present. Glaciers and snow at elevations higher than 5000 m a.s.l. in the western part of the catchment (Fig. 1B) cover an area of 125.8 km^2 (Wang and Dou, 1998; Song et al., 2014; Li et al., 2017a). According to a survey conducted in

2015, the pH of the lake water is 9.2 and the salinity is 29.5 g/L. Major anions and cations are $Cl^{-} > SO_4^{2-} > HCO_3^{-} > CO_3^{2-}$ and $Na^{+} > Mg^{2+} > Ca^{2+} > K^{+}$. The main carbonate mineral of the lake surface sediment is aragonite. Meteorological data from Shiquanhe Station (32.50° N, 80.08° E; altitude: 4279.3 m; 1971-2012, https://data.cma.cn/), 150 km to the west of Aweng Co, show that the mean annual temperature and precipitation are 0.68 °C and 69.11 mm, respectively. The temperature difference between summer (June, July and August) and winter (December, January and February) is more than 20°C and more than 85% of precipitation falls between May and September during the ISM season (Fig. 1C, Shiquanhe Station). Monthly mean temperature is above 0 °C between May and October (Fig. 1C), and the lake surface freezes in October and thaws in May. The oxygen isotope composition ($\delta^{18}O$) of the lake water was 0.2‰ in 2015. The slope of the local evaporation line (LEL) ($\delta^{18}O$ and $\delta^{2}H$) based on nine lake water samples and one ground water sample is lower than that of the regional (both Ngari and Aweng Co) meteoric water line (MWL, Fig. 1D), suggesting that evaporation has a significant influence on the lake water (Zhang et al., 2020). Li et al. (2017a) reconstructed Holocene mean annual air temperature and precipitation variations at low resolution using biomarkers from this lake, and they found a warm-wet early Holocene, cold and dry mid-Holocene, and a warm late Holocene.

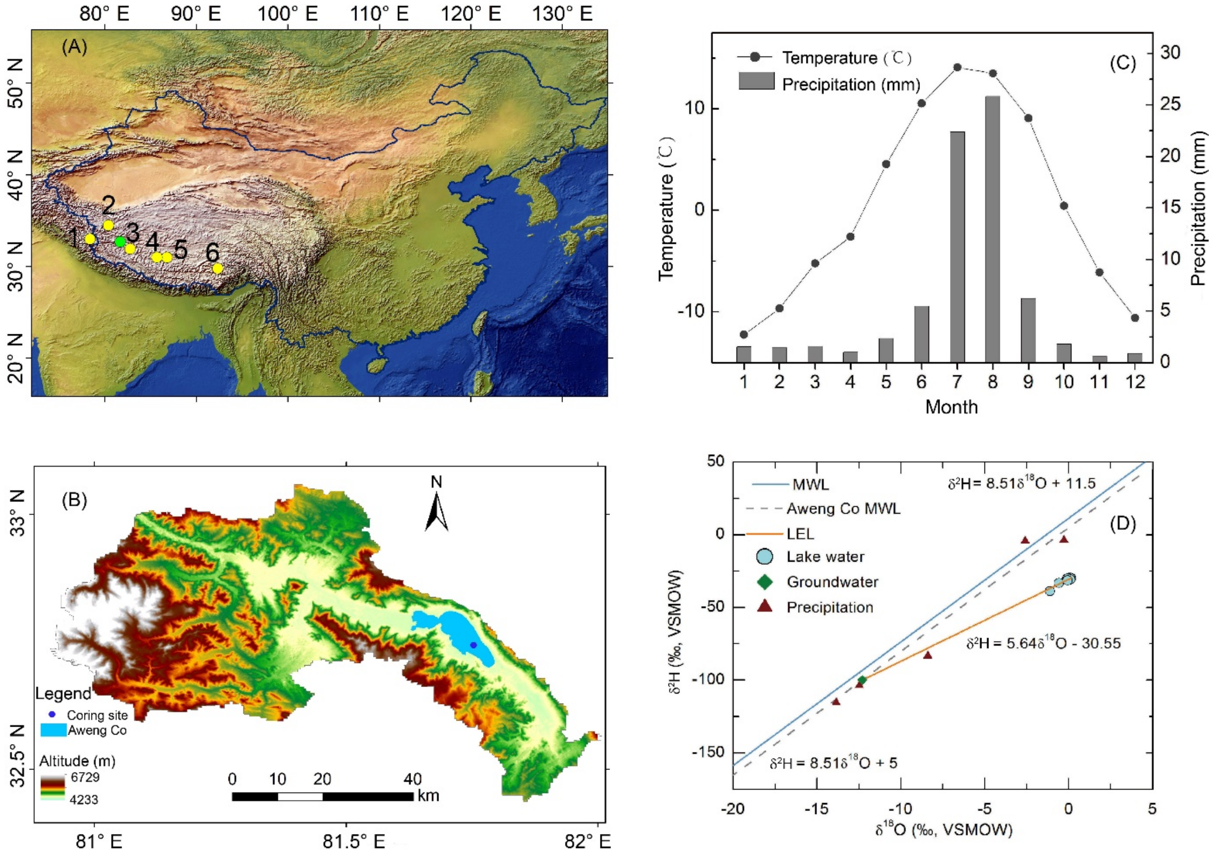

Fig. 1. The general situation of the study site. (A) shows the location of Aweng Co (the green dot) in the Tibetan Plateau. Yellow dots with numbers are sites of paleoenvironmental archives used for comparison: (1) Tso Moriri, (2) Longmu Co, (3) Baqan Tso, (4) Zhari Namco, (5) Tangra Yumco, and (6) Paru Co. (B) shows the catchment topography (modified from Li et al. , 2017a) and the coring site in Aweng Co (the black dot). (C) is the monthly mean temperature and monthly total precipitation in Aweng Co region between 1971-2012 (Shiquanhe Station, which is 150 km to the west of Aweng Co). (D) is the relationship between δ^2H and $\delta^{18}O$ in water showing the isotopic hydrology in Aweng Co region. The blue line is the local meteoric water line (MWL) from Ngari Station (Guo et al., 2017), the grey dashed line is the MWL of Aweng Co, and the orange line is the local evaporation line (LEL).

3 Materials and Methods

Two sediment cores (AWC2015A and AWC2015B) were retrieved from the central part of the lake (32.745° N, 81.757° E) at a water depth of 6 m using a UWITEC platform in July 2015. Core AWC2015B had an intact sequence with no obvious hiatuses and was analyzed, but AWC2015A was longer, so we used the part below 411.5 cm from AWC2015A (connected based on lithological change; Fig. A.1) giving a composite sequence (AWC2015) of 445 cm in length. The section 445-411.5 cm comprises grey-black silt (with shell fragments between 440 and 429 cm). Grey silt dominates from 411.5 to 175 cm, and between 175 and 70 cm, the sediment is brown-grey silt with laminated sections. The top 70 cm is predominantly grey-white silt. The core was split lengthwise into two halves: one was used for X-ray fluorescence (XRF) scanning, and then the two halves were sliced at 0.5 cm intervals yielding 890 samples that were freeze-dried for storage and analysis. No visible terrestrial plant remains were found in the sediments, therefore, bulk organic matter was used for radiometric dating. Sixteen samples of bulk organic matter and one sample of *Pisidium* shells (Table 1) were sent to Beta Analytic Inc., USA for accelerator mass spectrometry (AMS) ^{14}C dating. The top 15 cm of the core was dated by ^{210}Pb and ^{137}Cs using HPGe Gamma Spectrometry at Lanzhou University and a chronology established by the Constant Rate of Supply (CRS) model (Appleby and Oldfield, 1978).

Mineralogical components were determined by X-ray diffraction (XRD). Samples for XRD were ground using an agate mortar and pestle prior to analysis on a Panalytical X' pert Pro X-ray diffractometer with graphite monochromatized CuK radiation at 40 kV and 40 mA in the range of 5° to 75° (2θ). Data were processed using the X'Pert High Score Plus software package.

For grain size measurement, freeze-dried samples (~0.25g) were first reacted with 10% H_2O_2 to remove organic matter, and then with 10 mL 10% HCl to remove carbonates. Deionized water was added during the process. The acidic ions were rinsed by removing supernatant liquid after the sample solution had stood for 24h, then a dispersant solution ($(Na_2PO_3)_6$) was added to the residue, and sonicated for 5 minutes to facilitate dispersion (Peng et al., 2005). Grain size was then measured using a Malvern Mastersizer 2000. The range of the measurement was 0.02 – 2000 μm, and repeat error was less than 2%.

Fine sediments were wet sieved with 120-mesh (125 μm) and 360-mesh (40 μm) sieves and the fraction of < 40 μm was dried at 50 °C for 6 hours. The fraction > 125 μm was used for ostracod analysis. Three hundred ostracod shells were picked from each randomly selected sub-sample. If samples contained < 300 shells, all shells were picked from the sample (Mischke et al., 2010). A binocular microscope and scanning electron microscope (SEM) were used to identify the species, and shells used for isotope measurement were washed with ethanol (Mischke et al., 2010). Taxonomic identification of ostracod assemblages was conducted on 481 samples. The oxygen and carbon isotope composition of the fine fraction (carbonate) sediment ($\delta^{13}C_{carb}$ and $\delta^{18}O_{carb}$, 890 samples) and shells of *Limnocythere inopinata* ($\delta^{13}C_{ostra}$ and $\delta^{18}O_{ostra}$, 157 samples) were analyzed using a MAT 253 mass spectrometer (ThermoFisher Scientific) with an automated carbonate preparation device (Kiel IV). Four standards (NBS18, NBS19, GBW04405 and GBW04416) were measured every 10 samples. Analytical precision for $\delta^{13}C$ and $\delta^{18}O$ was < 0.1‰ and isotope data were reported relative to Vienna Pee Dee Belemnite (VPDB). The analyses were conducted at the Key Laboratory of Western China's Environmental Systems, Lanzhou University.

Samples for organic carbon isotope measurements were pretreated with 5% HCl for 16 h to remove carbonates, and then rinsed using deionized water until the pH was neutral, and dried at 50 °C for 6 hours. Organic carbon isotopes ($\delta^{13}C_{org}$) were measured using a Flash EA 1112 elemental analyzer and isotope ratio mass spectrometer (IRMS) at Lanzhou University, $\delta^{13}C_{org}$ was measured following the methods of Wang et al. (2014), with an analytical precision of < 0.1‰. We measured the organic carbon isotopes ($\delta^{13}C_{org}$) for 316 samples along the core sequence, at a resolution of 0.5 cm for the upper 17 cm, 1 cm from 17 to 160 cm, and 2 cm from 161 to 445 cm. Total organic carbon, total nitrogen and $\delta^{13}C_{org}$ were also measured on a Carlo Erba 1500 elemental analyzer connected to a VG Tripe Trap and Optima dual-inlet IRMS at the British

Geological Survey. Therefore, we have two sequences of $\delta^{13}C_{org}$ data at the same resolution for laboratory comparison. The values of $\delta^{13}C_{org}$ were calculated relative to the VPDB scale using within-run laboratory standard materials (calibrated to NBS standards). Analytical precision was better than 0.1‰. Total organic carbon/total nitrogen (C/N) atomic ratio was calculated by multiplying the C/N mass ratio by 1.167. Loss on ignition (LOI) was measured on 292 bulk samples (at a resolution of 2 cm for the upper 303 cm and 1 cm from 303 to 445 cm) at 550 °C in a muffle furnace for 4h to determine the organic matter content, the specific operation followed the method of Heiri et al. (2001). The results were then calculated to total organic carbon (TOC) according to the equation of TOC = 0.48 × LOI – 0.73 (Håkanson and Jansson, 1983). We used the TOC calculated from LOI at 550°C instead of the TOC from the elemental analyzer in later discussions in this paper, because samples analyzed by the elemental analyzer were pretreated with HCl, which can remove soluble organic matter.

4 Results and proxy explanations

4.1 AMS ^{14}C ages and the chronology

The AMS ^{14}C dating results are listed in Table 1. The age-depth relationship is plotted in Fig. 2A. The surface sample (0.5 cm of the core top) is dated to 3300 ± 30 ^{14}C yr BP (Table 1, Fig. 2A). The ^{210}Pb dating (CRS model, Fig. A. 2) suggests the age of the surface sediments is 0–2 years old (i.e., 2013–2015 CE). Therefore, these ^{14}C ages contain a significant reservoir effect (RE) that has to be properly assessed before establishing a reliable chronology. To assess the source of the 'old carbon' that caused the RE, we compared two samples at 413.5 cm. A *Pisidium* shell was dated to 10580 ± 40 ^{14}C yr BP and the bulk organic matter was dated to 10620 ± 40 ^{14}C yr BP (Table 1). Within dating errors, these two ages are actually the same, indicating that the 'old carbon' in both materials was mainly from the dissolved inorganic carbon (DIC) of the lake water as *Pisidium* sp. lives in water and uses DIC to form its shell. Old DIC in the lake water indicates that there is groundwater supplying the lake (Zhang et al., 2016a). Although we know that old carbon inputs (the RE) might change with time (indicated by reversed ages along the sequence), in the case of Aweng Co we are only able to obtain one RE for the sequence either using the ^{14}C age of the core top sample or the intercept of a regression equation applied to the age-depth sequence (Hou et al., 2012; Zhang et al., 2016a). In the 445-cm-long core AWC2015, we dated samples at 16 depths (Table 1) and most ^{14}C ages are in stratigraphic order (Fig. 2A), suggesting that one RE can be used for most of the ages in the sequence.

In assessment of the RE, we use the 'intercept method' (Hou et al., 2012; Zhang et al., 2016a) with a polynomial regression applied to ^{14}C ages in stratigraphic order. Based on observations of the age-depth distribution (Fig. A. 3), 3 reversed ages were not included in the regression (Fig. 2A) and the intercept of 3350 yrs is regarded as the RE of most ages (Table 1). For the 3 reversed ^{14}C ages (marked as A; orange dots in Fig. 2A), we first applied the equation in Fig. 2A to these depths to obtain a calculated age (A_D), the RE for ages at these depths was then calculated with the equation of $RE = A - A_D + 3350$ (Zhang et al., 2016a). Li et al. (2017a) reported the RE of the core AWC2011-2, near the core AWC2015, was 4066 yrs for the upper 309 cm, which is higher than the RE in the core AWC2015. We suggest this discrepancy is because the surface sample of the AWC2011-2 core was not dated by Li et al. (2017a) and the regression was dominated by old ages, in comparison to the ^{14}C ages in AWC2015 core. If a linear regression is applied to the upper 300 cm of core AWC2015 without the surface ^{14}C age, it would yield a RE of 3700 yrs (Fig. A. 4), which is higher than the current estimate of 3350 yrs, indicating the importance of dating the core top sample as a reference for RE evaluation.

After subtracting the REs from ^{14}C ages, we then calibrated the RE-corrected ages into calendar ages using IntCal 13 (Northern Hemisphere, Reimer et al., 2013) and established the age-depth model using Bacon, run in the R package (Fig. 2B; Christen and Pérez, 2010; Blaauw and Christen, 2011). According to our chronology, the age at the bottom of the core is 10.5 cal. kyr BP (1 kyr = 1000 yr). Therefore, AWC2015 covers sediments deposited since the early Holocene. The average data resolution is ~5 yr/sample for the upper 300 cm, and 20 – 30 yr/sample below 300 cm.

Table1 Results of radiocarbon (^{14}C) dating for AWC2015. The inversed dates are marked with * in the ^{14}C Ages column.

Sample No	Lab No	Depth (cm)	Material	$\delta^{13}C$ (‰)	^{14}C Ages (yr BP)	Reservoir effect (yr)	Corrected ^{14}C Age (yr BP)	Calibrated age (cal. yr BP±2σ range)
AWC15B-1	429459	0.5	TOC	–22.9	3300±30	3360	–60	—
AWC15B-50	429460	26.9	TOC	–21.5	4040±30*	3910	130	140±130
AWC15B-113	429461	60.7	TOC	–21.8	3990±30	3350	640	610±60
AWC15B-179	429462	89.5	TOC	–21.1	4420±30	3350	1070	990±60
AWC15B-242	429463	121	TOC	–21.2	4680±30	3350	1330	1240±60
AWC15B-301	429464	150.5	TOC	–22.0	5000±30	3350	1650	1550±130
AWC15B-358	429465	179	TOC	–22.0	5450±30	3350	2100	2070±80
AWC15B-420	429466	210	TOC	–22.3	5570±30	3350	2220	2240±90
AWC15B-481	429467	240.5	TOC	–23.0	5970±30	3350	2620	2750±30

AWC15B-530	429468	265	TOC	–23.4	5530±30*	2840	2690	2800±50
AWC15B-587	429469	293.5	TOC	–22.5	6230±30	3350	2880	3010±130
AWC15B-648	429470	324	TOC	–25.3	6170±30*	2880	3290	3520±70
AWC15B-720	429471	360	TOC	–23.5	7330±30	3350	3980	4470±60
AWC15B-787	429472	393.5	TOC	–24.2	8370±30	3350	5020	6050±130
AWC15B-827	429473	413.5	*Pisidium* shells	–3.3	10580±40	3350	7230	8060±90
AWC15B-827	429474	413.5	TOC	–25.6	10620±40	3350	7270	8090±80
AWC15B-887	429475	443.5	TOC	–23.3	13080±40	3350	9730	11070±170

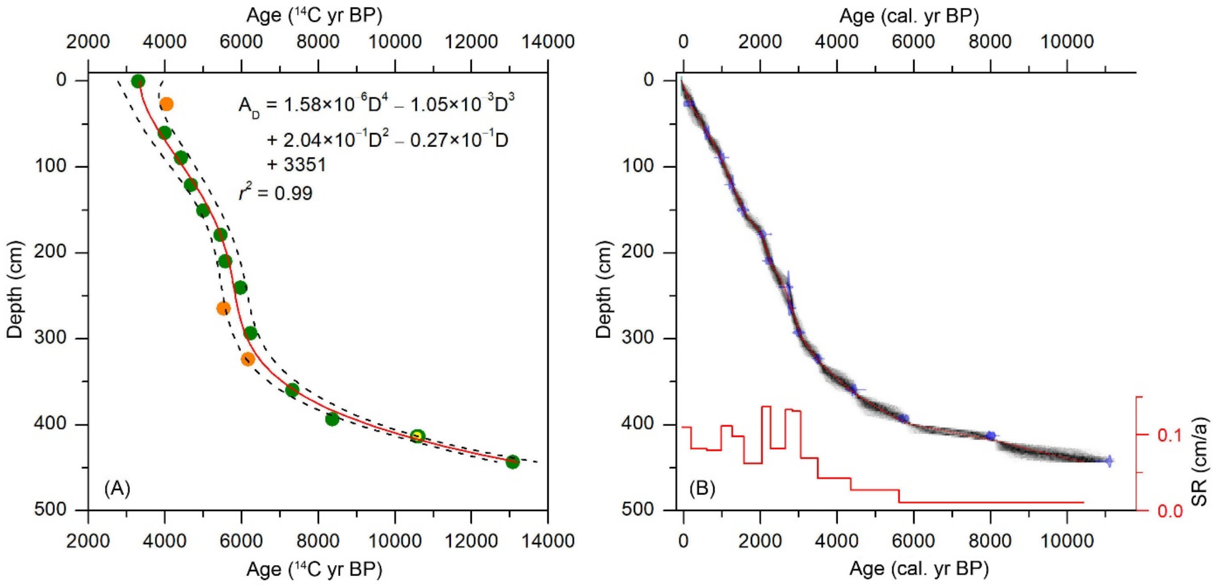

Fig. 2. Chronology and sedimentation rate of the core AWC2015. (A) shows the distribution of measured ^{14}C ages along the core. Green and yellow dots are used in the regression analysis with 95% confidence (black dashed lines). A_D represents the calculated ages in the depth D cm. The yellow dot was data derived from *Pisidium* shell at depth 413.5 cm. The orange dots are reversed ages not included in the regression. (B) is the calibrated age-depth model after subtracting the reservoir effect using Bacon in R for AWC2015. The red line shows variations in the sedimentation rate (SR).

4.2 Downcore variations of proxies and their paleoclimate/paleoenvironmental significance

4.2.1 Carbonate minerals indicated by XRD

The XRD analysis shows that aragonite is the dominant carbonate mineral (> 75%) with a small amount of calcite occurring through the core (Fig. 3A). Pure calcite was only detected at the bottom of the core. Between 370 and 300 cm (4.6 – 3.1 cal. kyr BP), the carbonate is dominated by dolomite (Fig. 3B). As aragonite precipitation requires higher Mg/Ca ratios of the lake water than calcite precipitation (Müller et al., 1972), the shift from calcite to aragonite in the lower part of the core indicates an increase of lake water salinity during the early- and mid-Holocene. Dolomite is a rare saline evaporite deposit in Holocene/modern lake sediments (Garrison and Graham, 1984; Roehl and Weinbrandt, 1985), which not only requires high lake water Mg/Ca ratios (Müller et al., 1972; Folk and Land, 1975; Gaines, 1980), but also microbial activity during its precipitation (Vasconcelos et al., 1995; Deng et al., 2010). Therefore, the carbonate mineralogy of AWC2015 indicates a fresher lake in the early Holocene, and afterwards the Mg/Ca ratios of the lake water increased until they favored aragonite, and dolomite deposition between 4.6 – 3.1 cal. kyr BP.

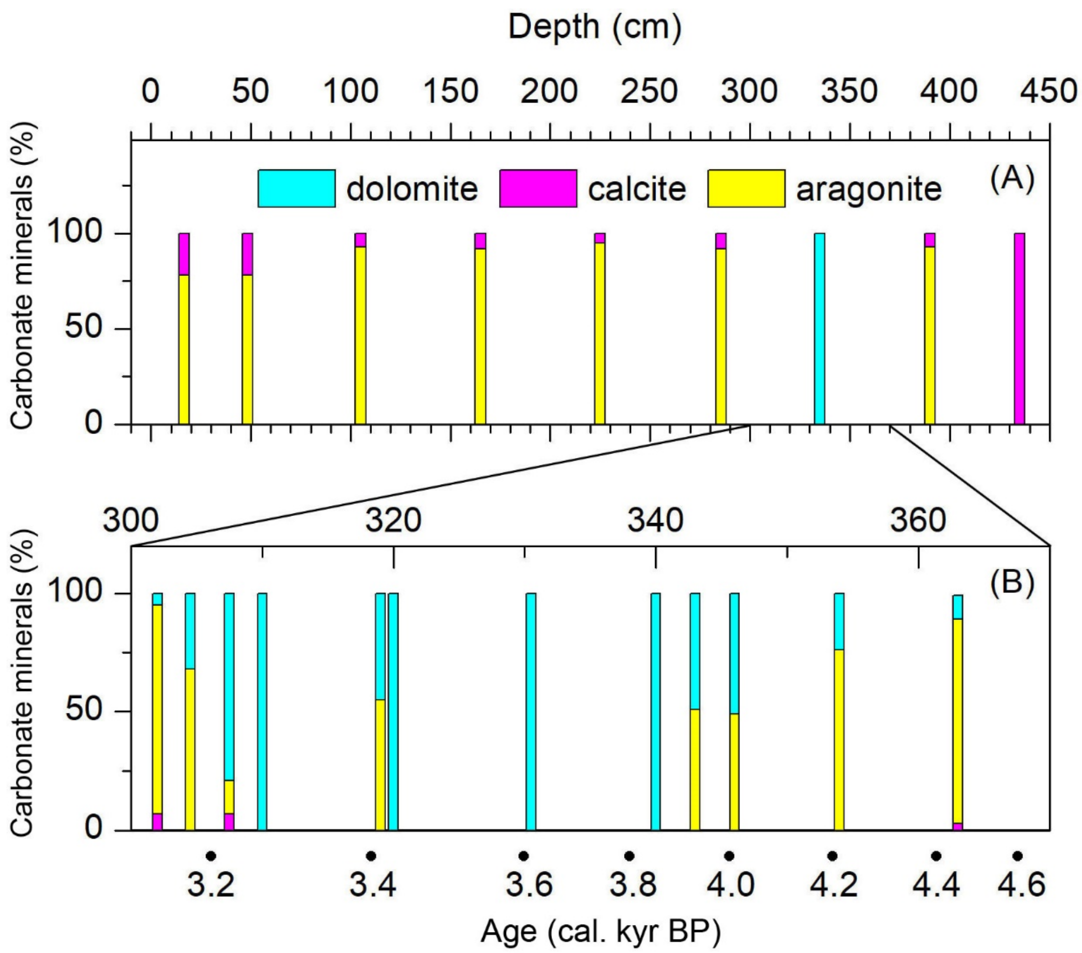

Fig. 3. Variations in the proportions of carbonate minerals along the whole core sequence (A) with details for the interval of 370 – 300 cm (B).

4.2.2 Ostracod assemblages

The shells of four ostracod species were preserved in the sediments (Fig. 4): *Limnocythere inopinata* (Baird, 1843), *Leucocytherella sinensis* Huang 1982, *Ilyocypris sebeiensis* Yang and Sun 2004, and *Fabaeformiscandona gyirongensis* Huang 1982, which is the same species as *Fabaeformiscandona danielopoli* Yin and Martens, 1997. Gastropod *(Pisidium* sp.) shells were also preserved in the sediments. *L.*

inopinata is a common ostracod species with a broad ecological tolerance (Meisch, 2000), which lives across a salinity range of 0 – 25 g/L (Griffiths and Holmes, 2000). *L. sinensis* is an endemic species of the TP (Xie et al., 2009), which can survive in fresh and brackish water with salinities of 0 – 20 g/L (Akita et al., 2016) but apparently prefers relatively cold environments. *I. sebeiensis* is usually regarded as an indicator of running water (Mischke et al., 2014). *F. gyirongensis* is a brackish-lacustrine species which lives in water salinity ranges of 0.1 – 1.3 g/L (optimum of 0.3 g/L; Mischke et al., 2003) and prefers to live in flowing water (Mischke et al., 2007).

The abundances of *L. inopinata*, *L. sinensis* and *F. gyirongensis* are high near the base of the core and then they decrease abruptly to fewer than 20 valves/g below 426 cm (Fig. 4). Afterwards all species increase to their highest abundances (except *L. inopinata*) and subsequently decrease gradually. *F. gyirongensis* and *Pisidium* sp. disappear from the record around 380 cm and *L. sinensis* and *I. sebeiensis* disappear around 342 cm (Fig. 4). Above 342 cm, only *L. inopinata* is rarely present, reaching its highest abundance (> 300 valves/g) between 250 – 200 cm, before disappearing around 176 cm (Fig. 4).

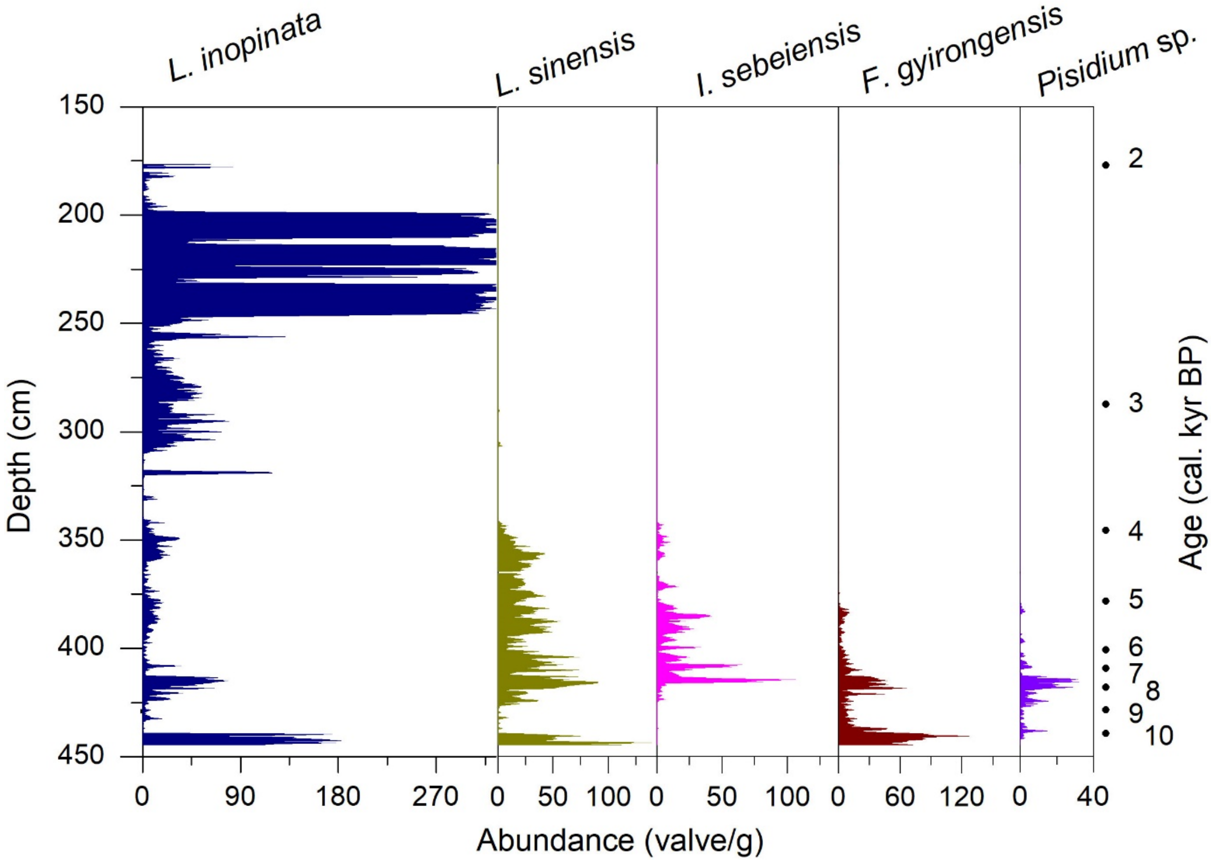

Fig. 4. Abundances (in valves per gram of dry sediment) of ostracod taxa and of the gasteropod *Pisidium* sp. in the AWC2015 sequence. The numbers on the right side indicate calibrated ages (in cal. kyr BP).

4.2.3 $\delta^{18}O$ of carbonate and ostracod shells

$\delta^{18}O_{carb}$ through the core varies from –7.4‰ to +3.2‰ with a range of 10.6‰ (Fig. 5A). Low $\delta^{18}O_{carb}$ values (<–4‰) occur below 410 cm and shift towards more positive values up the core. Frequent fluctuations to higher $\delta^{18}O_{carb}$ occur above 250 cm (Fig. 5A). In addition, the $\delta^{18}O_{carb}$ are very similar to $\delta^{18}O_{ostra}$ values from the bottom to ca. 200 cm, confirming the endogenic nature of the carbonate. Generally, the isotope composition of lacustrine carbonates ($\delta^{18}O_{carb}$ and $\delta^{18}O_{ostra}$) is determined by the lake water isotopic composition and water temperature (Leng and Marshall, 2004). The influence of temperature could be assessed by the equilibrium isotope fractionation between carbonate and lake water temperature (–0.24 ‰/°C; Craig, 1965). Assuming no precipitation change, our observed change of 10.6‰ in $\delta^{18}O_{carb}$ would require more than 40 °C of temperature change, which is beyond the scope of any past estimates from the TP (Zhao et al., 2013; Hou et al., 2016). Therefore, we infer that the $\delta^{18}O_{carb}$ and $\delta^{18}O_{ostra}$ are mainly controlled by the isotope composition of the lake water ($\delta^{18}O_{w}$), which is controlled by the composition of the water supplied to the lake and its enrichment by evaporation.

According to the result of the hydrological balance model described in Zhang et al. (2020), currently the main water supplies to Aweng Co are regional precipitation (50%) and glacier/snow melt (50%). In more recent times, due to global warming, we would expect more glacier melt water to flow into the lake, resulting in a higher proportion of melt water to the total supply today than earlier in the Holocene. This would also cause lower $\delta^{18}O_{w}$ as seen in the upper 20 cm of the core (Fig. 5A). Before the global warming of recent centuries, when glacier discharge was relatively lower, precipitation would have been a more dominant component of the lake water budget and $\delta^{18}O_{w}$ is more likely to have followed the pattern of changes in $\delta^{18}O$ of the precipitation. The isotope composition of precipitation and lake water in the Aweng Co region shows that the gradient of the LEL is lower than that of the LMWL (Fig. 1D), indicating that evaporation is an important factor that drives the water isotope change in the lake, as verified by the hydrological balance model that shows evaporation accounts for ~60% of water loss (Zhang et al., 2020). Therefore, at present, the input and evaporation (I:E) ratio is probably, the main driver of $\delta^{18}O_w$ and $\delta^{18}O_{carb}$. In this study, we do not correct for the small fractionation differences between aragonite and calcite as the impact of this is much smaller (~0.6 ‰; Grossman and Ku, 1986) than the range of our $\delta^{18}O_{carb}$ data (10.6‰; Fig. 5A). In addition, the $\delta^{18}O_{carb}$ data in the interval of dolomite precipitation are not discussed because of possible incomplete reactions of carbonate with phosphoric acid during the automated analysis procedure.

4.2.4 Organic variables

The organic matter content (from LOI) is < 8% below 376.5 cm, and then shifts to higher values above 376.5 cm. High frequency variations occur in the upper 300 cm (Fig. 5B). C/N ratios range from 9.9 to 13.4 below 300 cm, and are < 10 (mean C/N = 9.2) above 300 cm (Fig. 5C). C/N ratios of algae are generally between 4 and 10, and C/N ratios of terrestrial material is generally higher than 20 (Meyers and Ishiwatari, 1993). The C/N ratios in the core suggest that the organic matter preserved in the sediment is a mixture of terrestrial plants and algae from 445 to 300 cm, and dominated by algae thereafter (mean C/N = 9.2).

$\delta^{13}C_{org}$ increases from −26‰ to −21‰ at 150 cm, then decreases to −23‰, and finally reaches around −22‰ (Fig. 5D). The organic matter in Aweng Co sediments is probably from both terrestrial and aquatic primary producers. The terrestrial plants in the catchment have mean $\delta^{13}C_{org}$ value of −24.6‰ and the $\delta^{13}C_{org}$ of the aquatic plants is > −24‰ (when the C/N ratio is < 10). The study carried out by Zhang et al. (2016b) shows that in lake sediments from western China, $\delta^{13}C_{org}$ of phytoplankton (−30‰ to −23‰) and benthic algae (−24‰ to −16‰) are different, suggesting that the aquatic organic matter in AWC2015 could have been dominated by benthic algae. Therefore, the $\delta^{13}C_{org}$ variations reflect the proportional variations of terrestrial plants and benthic algae below 300 cm (when C/N > 10). Afterwards, when the benthic algae were the main source of organic matter as suggested from C/N ratio, the $\delta^{13}C_{org}$ was possibly affected by the carbon source and productivity variations. Due to degradation of the organic matter on the sediment surface before being buried, more ^{12}C from degraded organic matter would be preferentially assimilated (Meyers and Teranes, 2001) and the $\delta^{13}C_{org}$ values would be lower when the productivity was higher, as demonstrated by the overall inverse relationship between TOC and $\delta^{13}C_{org}$ (Fig. 5).

4.2.5 Grain size

The mean grain size of the sediment in core AWC2015 is generally < 32 μm below 350 cm (Fig. 5E), it increases with fluctuations to higher values of ~60 μm at ~240 cm, then decreases gradually to relatively stable values (Fig. 5E). Comparisons of the 20-point-smoothed curve and the $\delta^{18}O_{carb}$ variations show that low $\delta^{18}O_{carb}$ phases coincided with smaller mean grain size values, indicating when the I:E ratio (or effective humidity) was higher, the particles in the lake center were finer; and vice versa. Therefore, the overall variations of mean grain size can reflect lake level change to some extent. When the lake level was higher, only fine-grained particles could reach the lake center, whereas, stronger hydrodynamics allowed the coarser particles to be deposited in the lake center during lower lake levels.

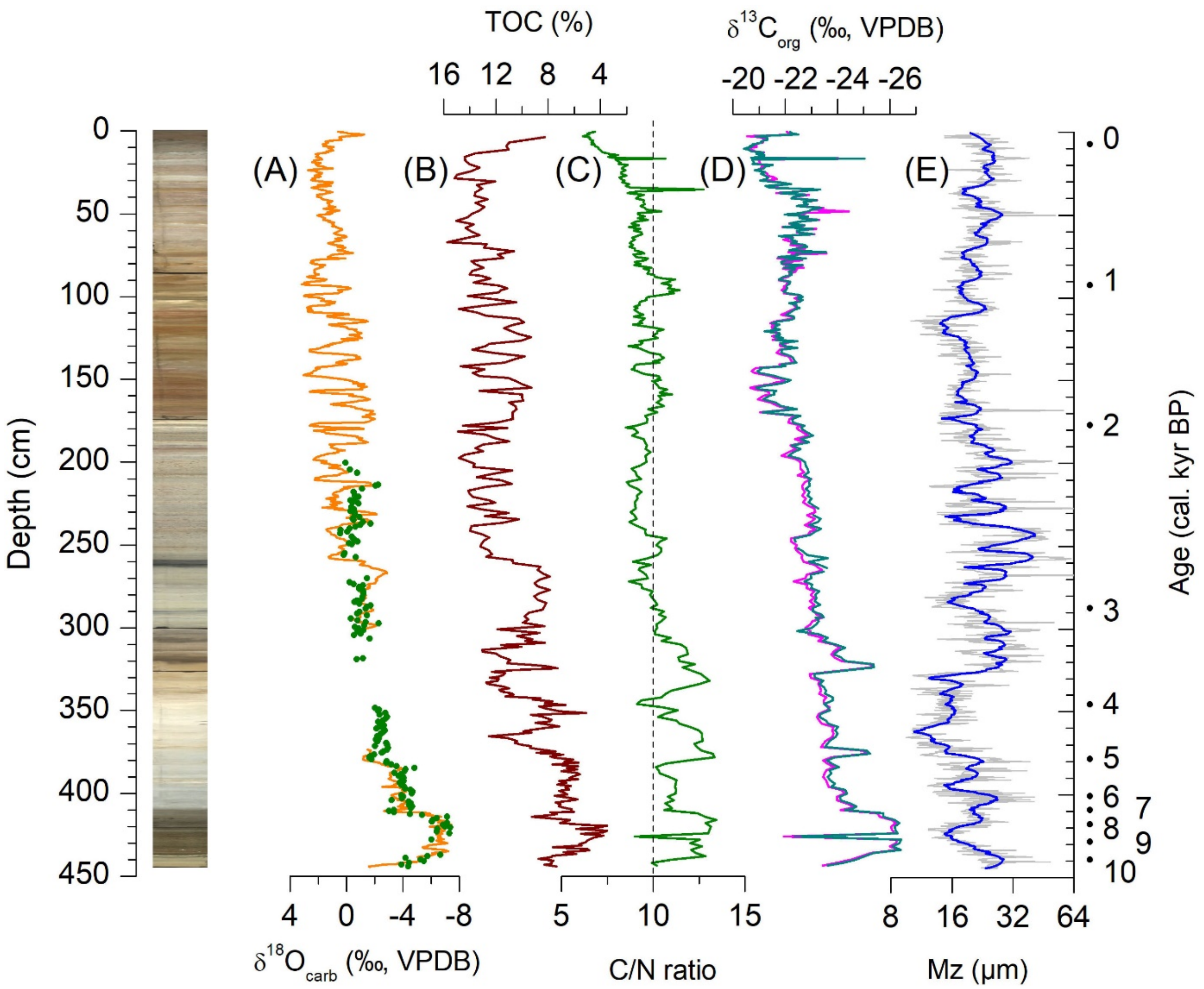

Fig. 5. Geochemical proxies from core AWC2015. (A) shows $\delta^{18}O$ variations of endogenic carbonates (solid lines) and ostracod (*L. inopinata*) shells (green dots). (B) is the TOC calculated from LOI at 550 °C. (C) – (D) represent C/N ratio and $\delta^{13}C_{org}$ variations (the light blue and magenta lines represent the data from BGS and the data from Lanzhou University, respectively). (E) is mean grain size (Mz) variation. The numbers on the right side indicate calibrated ages (in cal. kyr BP).

5 Discussion

5.1 Climatic and environmental change during the Holocene in the western Tibetan Plateau

We use the $\delta^{18}O_{carb}$ and $\delta^{18}O_{ostra}$ as climate indicators and organic variables (TOC, C/N, $\delta^{13}C_{org}$) as the environmental indices to reconstruct climatic and environmental changes in the Aweng Co region during the Holocene. Four phases can be identified based on their reconstructed hydro-climatic characteristics, and terrestrial and aquatic environment responses to these changes are explored below.

Phase 1: 10.5 – 7.3 cal. kyr BP (445 – 411.5 cm)

Before 7.3 cal. kyr BP, $\delta^{18}O_{carb}$ and $\delta^{18}O_{ostra}$ suggest that climate was the wettest and high precipitation led to high lake levels and low salinity, favoring the growth of the freshwater ostracod species *F. gyirongensis* and *Pisidium* sp. (Fig. 4). *L. sinensis* prefers living in relatively cold environments, while *F. gyirongensis* prefers a flowing water environment (Mischke et al., 2003, 2014). When the lake level was higher, the water at the lake bottom became still, resulting in a reduction in their abundances from 10 to 8.2 cal. kyr BP.

The C/N ratio was <10 during the interval around 8.8 cal. kyr BP, indicating that organic matter was mainly from benthic algae with a $\delta^{13}C_{org}$ of around −22‰ (Fig. 5). The $\delta^{13}C_{org}$ of modern plants and soil in the catchment are around −24.6‰ (mean of the terrestrial plants) and −23.9‰, respectively. Based on the relationship between $\delta^{13}C_{org}$ of C_3 plants and precipitation (–1.1‰/100 mm) in NW China (Liu et al., 2005), and assuming that precipitation in the early Holocene was 200 mm more than that in the late Holocene (Li et al., 2017b); the $\delta^{13}C_{org}$ of terrestrial plant material in the early Holocene should have been around –26‰. Using the above assumptions, terrestrial plants and benthic algae probably contributed ~82% and ~18% to the TOC, respectively. More terrestrial C_3 plants would be expected during periods of higher precipitation. The pollen record from Bangong Co, which is located in the same region as Aweng Co, also showed the *Artemisia/Amaranthaceae* (*Ar/Am*) ratio was the highest in the early Holocene (Van Campo et al., 1996). However, the productivity of the benthic algae was very low as inferred from the TOC and C/N ratio in this phase, which might be caused by limited sunlight reaching the lake bottom when the lake level was high.

Phase 2: 7.3 – 5.0 cal. kyr BP (411.5 – 379.5 cm)

Although the climate became more arid than the previous phase as indicated by higher $\delta^{18}O_{carb}$ and $\delta^{18}O_{ostra}$ values, the lake water was probably still fresh as indicated by the abundance of *F. gyirongensis* and *Pisidium* sp. (Fig. 4). The gradual decline in all ostracod species suggests the lake water salinity increased and exceeded 1.3 g/L when the ostracod species *F. gyirongensis* and *Pisidium* sp. disappeared around 5.0 cal. kyr BP (Fig. 4). Reduced precipitation would limit both the growth of C_3 plants in the catchment and subsequent transport of organic matter of terrestrial origin to the lake in this phase. The higher TOC and lower C/N ratio indicate the productivity of the benthic algae was higher, possibly as a result of lower lake levels, allowing illumination of a greater proportion of the lake bottom when the climate became drier.

Phase 3: 5.0 – 3.1 cal. kyr BP (379.5 – 300 cm)

Dolomite in this phase indicates the climate was much drier, the lake water salinity increased further and the brackish water species *L. sinensis* and *I. sebeiensis* vanished around 3.9 cal. kyr BP and only *L. inopinata* remained (Fig. 4). Increased TOC values during 3.9 – 3.2 cal. kyr BP (Fig. 5B) were possibly as a result of low lake level under a dry climate.

Phase 4: 3.1 cal. kyr BP to present (above 300 cm)

In this phase, $\delta^{18}O_{carb}$ values continue a general trend to more positive values and become more variable, implying the climate was continuing to become more arid. Increased $\delta^{18}O_{carb}$ variability may have been due to the increased isotopic sensitivity of a smaller water body (e.g. Leng and Marshall, 2004; Steinman et al., 2010a, b). The driest climate since the early Holocene caused even higher lake water salinity, leading to the disappearance of *L. inopinata* around 2 cal. kyr BP (Fig. 4). Sparse vegetation in the catchment limited the input of terrestrial organic matter (C/N ratios of mostly <10; Fig. 5C). In addition, the eggs of brine shrimp were found in the sediment after 2 cal. kyr BP, demonstrating that the lake water salinity was much higher and not suitable for *L. inopinata*. Although the freezing and thawing effect still led to soil erosion (Sun et al., 2008), the reduced precipitation probably led to lower lake levels, less transport of nutrients from the soil, and more light reaching the lake bottom thereby facilitating colonization by benthic algae, as demonstrated by the higher TOC (Fig. 5B). The high frequency variation of TOC (Fig. 5B) was possibly caused by an unstable climate indicated by $\delta^{18}O_{carb}$ and $\delta^{18}O_{ostra}$ variations. Higher content of organic matter corresponds to more positive $\delta^{18}O_{carb}$ values (Fig. 5; Fig. A. 5), indicating that benthic algae in the lake grew better in a more evaporated (shallower) lake.

Overall, data from Aweng Co show that the terrestrial and aquatic ecosystems in this region were highly sensitive to climate change during the Holocene. When the climate was wet before 5.0 cal. kyr BP, lake water was fresh, there was high biomass of terrestrial plants in the catchment, and the benthic algal habitats received less sunlight as a result of high lake level, leading to low algal biomass. After 5.0 cal. kyr BP, the climate was drier, lake water salinity increased, especially after 3.1 cal. kyr BP, and we suspect that the catchment vegetation became sparse, while there was a further expansion in benthic algal productivity when the lake was shallow.

5.2 Comparison with regional records

The speleothem $\delta^{18}O$ record from Qunf Cave in Oman (Fleitmann et al., 2003, 2007), the hydrogen isotope (δ^2H) of leaf wax (long-chain n-alkanes) in Paru Co on the TP (Bird et al., 2014) and the synthesized moisture index from the ISM region (Zhang et al., 2011) are compared with the $\delta^{18}O$ records from Aweng Co (see Fig. 6). The speleothem $\delta^{18}O$ records from Qunf Cave are thought to faithfully record the evolutionary history of the ISM (Fleitmann et al., 2003, 2007), with maximum ISM rainfall in the early Holocene, followed by a decrease after 5 cal. kyr BP (Fig. 6A). The well-dated hydrogen isotope (δ^2H) of long-chain (C_{27}, C_{29}) n-alkanes (leaf wax) from Paru Co (Bird et al., 2014), also an indicator of ISM variability, shows a similar pattern (Fig. 6B). The isotope records from Aweng Co are in good agreement with the well-dated records of humidity variations in the southern Tibetan Plateau and ISM region. In addition, δ^2H of *n*-alkanoic acids at

Aweng Co (C_{26}, C_{28}) from the core AWC2011-2 showed a strong intensity of the Indian summer monsoon and a high amount of precipitation before 5.5 cal. kyr BP (Li et al., 2017a). The $\delta^{18}O_{carb}$ in Aweng Co is also consistent with another record of $\delta^{2}H$ of *n*-alkanoic acids from Bangong Co in the western TP, 150 km northwest of Aweng Co, where the ISM was strong until around 4.5 cal. kyr BP (Hou et al., 2017). Furthermore, the synthesized moisture indices based on $\delta^{18}O_{carb}$ records in the monsoon region of China (Fig. 6G; Zhang et al., 2011) also showed that humidity indices tended to be lower than 0.5 around 5 cal. kyr BP, suggesting lower ISM rainfall after 5 cal. kyr BP. The consistency of $^{18}O_{carb}$ in Aweng Co with records from the ISM region (Fig. 6) demonstrates that ISM intensity could have been driving lake hydrology of Aweng Co. Such a pattern of variation is completely different from that of the moisture change in the region dominated by the westerlies, which is thought to be persistently wet since the early Holocene (Wang et al., 2013; Chen et al., 2016). Therefore, the climate in the western Tibetan Plateau was mainly controlled by the ISM during the Holocene, which was driven by solar insolation variations (Fleitmann et al., 2007).

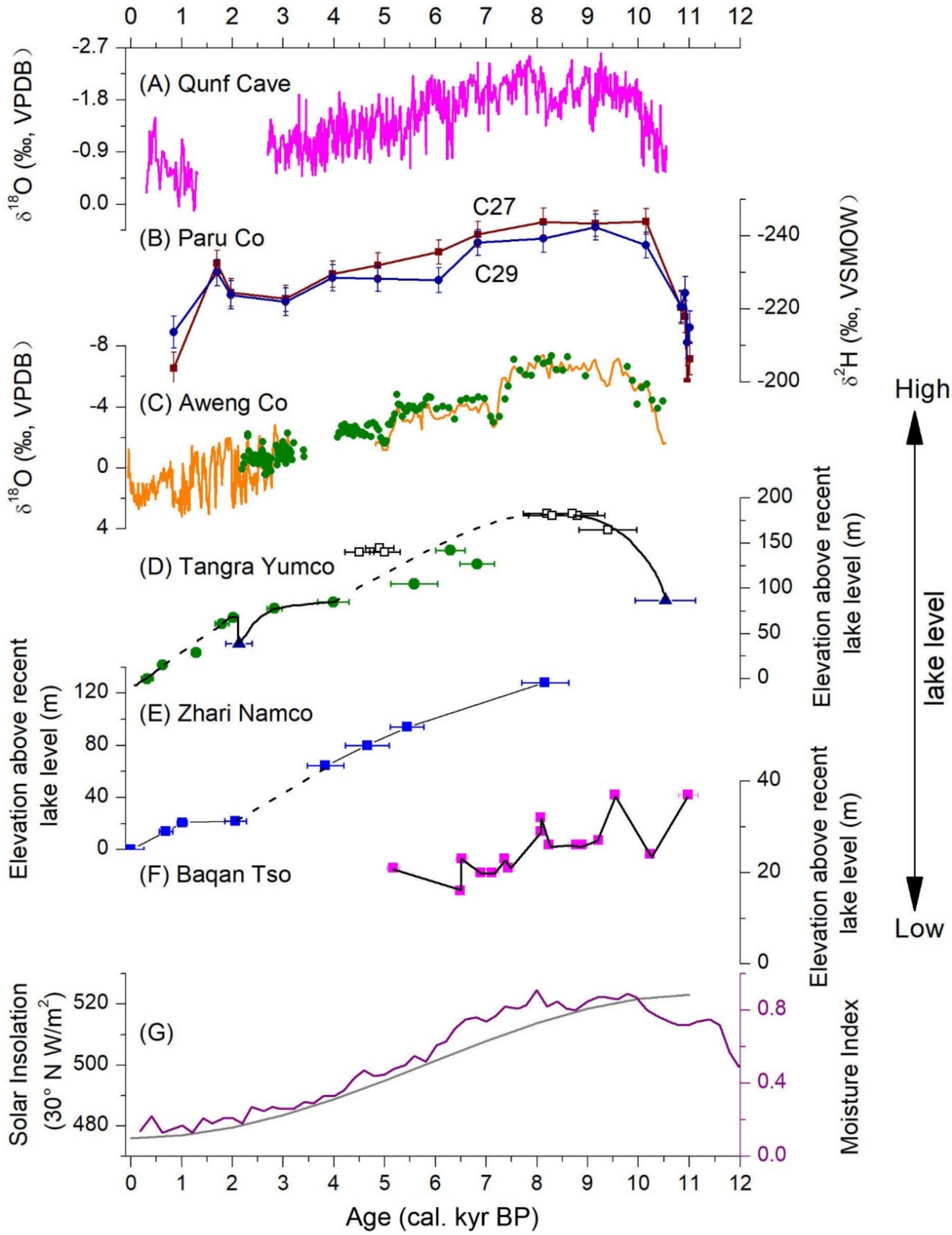

Fig. 6. Comparisons of the proxies from Aweng Co with records from ISM region. (A) is the $\delta^{18}O$ record from Qunf Cave (Fleitmann et al., 2003, 2007). (B) shows δ^2H of leaf wax from Paru Co (Bird et al., 2014). (C) the orange line and green dots are the $\delta^{18}O$ of carbonate and ostracod shells from the core of Aweng Co,

respectively. (D) – (F) the lake level change of Tangra Yumco (Kong et al., 2011; Rades et al., 2013, 2015; Ahlborn et al., 2015), Zhari Namco (Chen et al., 2013) and Baqan Tso (Huth et al., 2015). (G) The purple curve and the grey line are the synthesized moisture index from ISM region and the solar insolation at 30°N (redrawn from Zhang et al., 2011), respectively.

The lake level of Aweng Co inferred from $\delta^{18}O_{carb}$ was high in the early Holocene before 7.3 cal. kyr BP, and decreased to the lowest in the late Holocene. Such a pattern of lake level variation in Aweng Co is consistent with the regional lake level variations indicated by elevations of paleo-shorelines preserved beside lakes in the southern TP, including Tangre Yumco (Fig. 6D; Kong et al., 2011; Rades et al., 2013, 2015; Ahlborn et al., 2015), Zhari Namco (Fig. 6E; Chen et al., 2013), Baqan Co (Fig. 6F; Huth et al., 2015), Ngangla Ring Tso (Hudson et al., 2015) and Peiku Co (Wünnemann et al., 2015). All these paleo-shorelines with reliable chronologies in the ISM-influenced region clearly showed that lake levels were high in the early Holocene and declined continuously with small fluctuations during the mid- and late-Holocene. In addition, the lake area/watershed area ratio, a better measure of the hydrological budget for closed basins, from Seling Co and Lagkor Co in the southern TP, was highest before 5 cal. kyr BP (Liu et al., 2013), suggesting that precipitation (or effective precipitation) was high before 5 cal. kyr BP. Therefore, the coeval declining trend of all these records demonstrates that solar insolation variations play important roles in determining hydrological change in the southern and western TP. The insolation-controlled intensity of the ISM was the highest with abundant precipitation in the early Holocene, resulting in high lake levels (Fig. 2B) as mainly fine minerogenic particles were deposited in the lake center due to the long distance of transportation (Sun et al., 2001; Opitz et al., 2012). With declining solar insolation, especially after 5 cal. kyr BP, the ISM brought less precipitation (Fleitmann et al., 2003) and the lake level dropped. Therefore, coarser particles could reach the lake center with strong water level fluctuations resuspending marginal sediments and shortened transport distances.

Comparisons of the $\delta^{18}O_{carb}$ variations with the possible climate drivers (Fig. A. 6) show that $\delta^{18}O_{carb}$ variations are generally consistent with the Indo-Pacific sea surface temperature (SST) changes, suggesting that high Indo-Pacific SST leads to relatively wet climate (low $\delta^{18}O_{carb}$ values) in the western TP and vice versa. Centennial-scale weaker monsoon periods recorded in Ngamring Tso were also linked to cooler Indo-Pacific SST (Conroy et a., 2017), suggesting that the climate change in the western TP at centennial scale in the late Holocene was driven by the Indo-Pacific SST to a large extent. Centennial-scale climate change in the ASM region has also been linked with solar activity in the late Holocene (Tan et al., 2018). The power spectrum analysis of $\delta^{18}O_{carb}$ in Aweng Co shows three dominant cyclicities of 66-yr, 43-yr and 22-yr in the past 3.1 kyr (Fig. A. 7), consistent with solar activity periodicities (Stuiver and Braziunas, 1998). Therefore, we conclude that the high-frequency variations of the climate in the western TP in the late Holocene was driven by solar activity and Indo-Pacific ocean-atmosphere circulation synchronously.

5.3 The northern limit that ISM could influence in the western TP during the Holocene

Two lakes located in the western TP, together with Aweng Co (Fig. 7) were chosen to detect how the ISM could influence precipitation change in the western TP during the Holocene. The $\delta^{18}O_{carb}$ from Aweng Co (32.7° N, 81.7° E, this research) and Tso Moriri (33° N, 78.4° E) both recorded regional effective humidity change (Mishra et al., 2015). The paleo-shorelines from Longmu Co (34.5° N, 80.3° E), the most northerly record from the western TP, provides solid evidence of high lake levels, and thus could reflect effective humidity variations (Liu et al., 2016). Together with the dated paleo-shorelines at Longmu Co (Fig. 8; Liu et al., 2016) and $\delta^{18}O_{carb}$ from Aweng Co reveal that the lake level was the highest before ~7.3 cal. kyr BP, and declined afterwards. The $\delta^{18}O_{carb}$ from Tso Moriri shows that the climate in these regions was the wettest before 5 cal. kyr BP and became drier afterwards (Fig. 8; Mishra et al., 2015). The climate in the region influenced by the ISM was relatively wet in the early and mid-Holocene, and shifted to dry conditions in the late Holocene (Zhang et al., 2011). Therefore, we tentatively infer that the ISM reached the position of 34.5°

N in the western TP during the early Holocene based on the currently published data (Fig. 7). With the southerly migration of the ITCZ, the westerlies moved southwards synchronously to the position of the modern TP shear line (red dashed line in Fig. 7), where the atmospheric water vapor from the westerlies and the ISM converge (Wang et al., 2005). Monthly-clustered back trajectory analysis showed that water vapor in Ngari (33.39° N, 79.70° E; green square in Fig. 7) includes local vapor and air masses transported by the westerlies and ISM (Guo et al., 2017). Therefore, the moisture in the zone of 30.6° N – 34.5° N was possibly from both the ISM and the westerlies during the Holocene in the western TP (Fig. 7), with varying contributions depending on the intensity of the ISM.

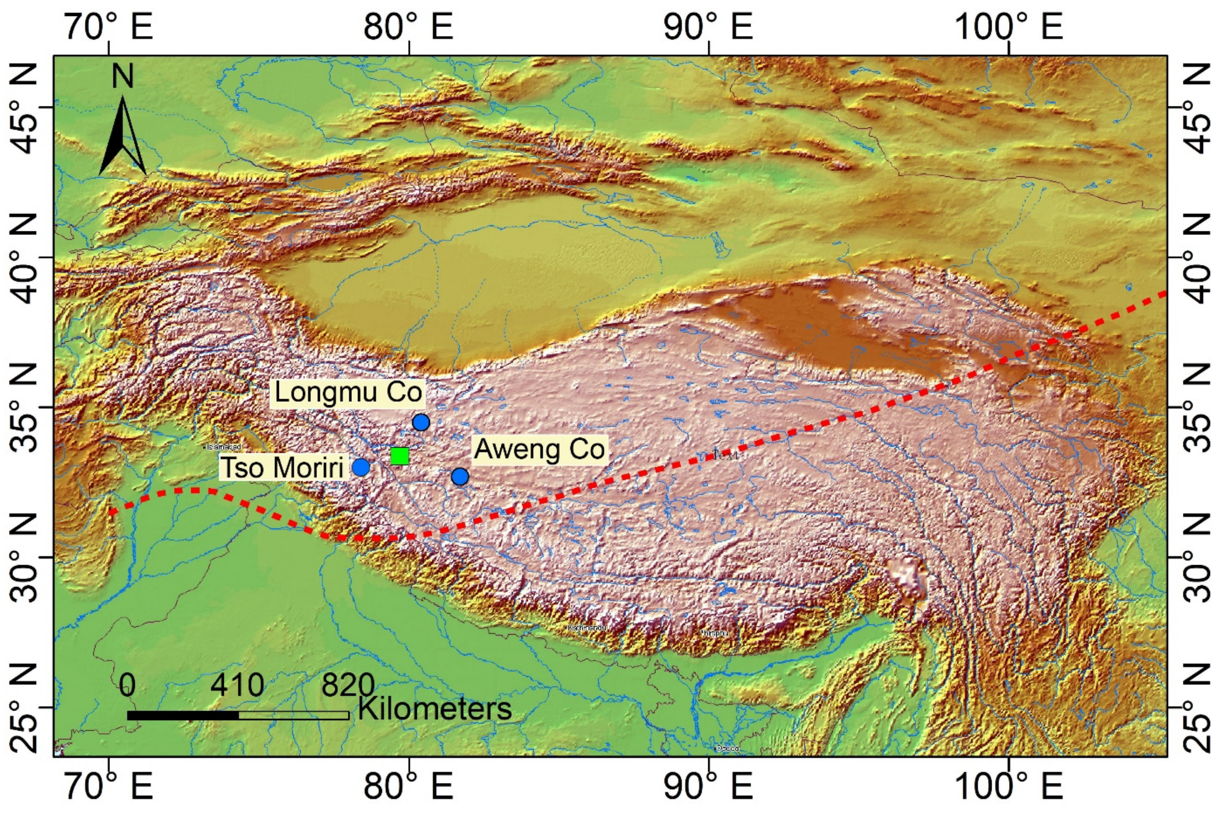

Fig. 7. The region that the ISM could influence during the Holocene in the western TP. The green square is

the location of Ngari Station, and the red dashed line is the modern TP shear line, which separates water vapor from the westerlies and ASM (Wang et al., 2005).

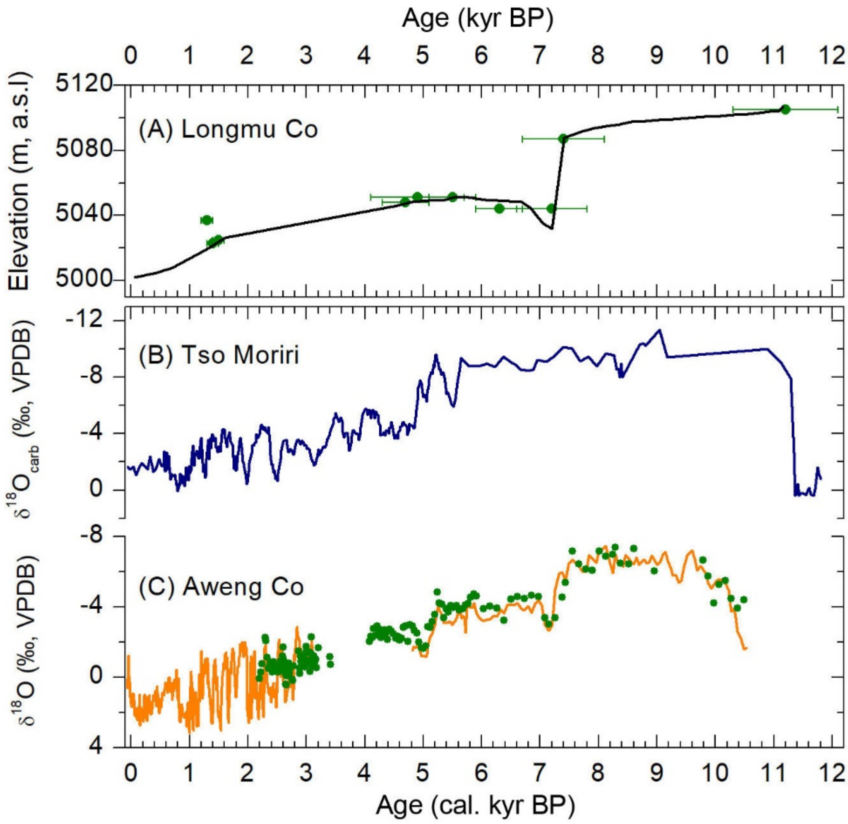

Fig. 8. Comparisons of lake sediment records in the western TP. (A) Paleo-shoreline record from Longmu Co (Liu et al., 2016). (B) $\delta^{18}O_{carb}$ record from Tso Moriri (Mishra et al., 2015). (C) The orange line and green dots are the $\delta^{18}O$ of carbonate and ostracod shells from the core AWC2015, respectively (this study).

6 Conclusions

Holocene climate and environmental change history are reconstructed using multiple proxies from lake sediments in Aweng Co in the western Tibetan Plateau. We conclude that:

(1) This region was influenced by the ISM throughout the Holocene. Precipitation was relatively high before 5.0 cal. kyr BP and conditions became more arid thereafter, resulting in relatively high terrestrial plant productivity in the early Holocene before 7.3 cal. kyr BP and low terrestrial biomass after 5.0 cal. kyr BP. Benthic algal biomass was low in the early Holocene and became higher in the late Holocene, resulting from increasing sunlight exposure of the lake bottom when the lake level was lower. The terrestrial-aquatic ecosystem in the arid region of the western Tibetan Plateau was highly sensitive to climate change.

(2) Climate change in the western TP was controlled by solar insolation during the Holocene in general, whereby, solar activity and the Indo-Pacific ocean-atmosphere circulation play important roles in driving the high-frequency fluctuations of the climate in the last 3.1 kyr.

(3) Lake level change inferred from $\delta^{18}O_{carb}$ variations in Aweng Co is consistent with the existing paleo-shoreline records in the southern TP controlled by ISM evolution, with high lake levels in the early Holocene and decline thereafter, which could be confirmed by dating the paleo-shorelines around the lake in the future.

(4) Comparisons of lake records located in the western TP suggest the ISM reached 34.5° N in the western TP in the early Holocene, when ISM intensity was at a maximum and retreated gradually to 30.6° N in the late Holocene. Given the limited published records in the western TP, establishing the specific northern

boundary of ISM influence during the Holocene requires further reconstructions from more sites in the future.

Acknowledgments

This study is supported by the National Natural Science Foundation of China (NSFC 41771212) and Fundamental Research Fund for the Central Universities (lzujbky-2017-it81). We would like to thank Mingda Wang, Yaping Yang and Erlei Zhu for assisting with field work, Pingyu Zhang, Xueli Cui and Xueyang Ma for lab work. We thank Adam Hudson, the anonymous reviewer and Patrick Rioual (the editor) for constructive comments/suggestions which improved the manuscript. The authors have no conflict of interest to declare.

References

Ahlborn, M., Haberzettl, T., Wang, J., Fürstenberg, S., Mäusbacher, R., Mazzocco, J., Pierson, J., Zhu, L., Frenzel, P., 2015. Holocene lake level history of the Tangra Yumco lake system, southern-central Tibetan Plateau. Holocene 26, 176–187. https://doi.org/10.1177/0959683615596840

Akita, L.G., Frenzel, P., Wang, J., Börner, N., Peng, P., 2016. Spatial distribution and ecology of the Recent Ostracoda from Tangra Yumco and adjacent waters on the southern Tibetan Plateau: A key to palaeoenvironmental reconstruction. Limnologica 59, 21–43. https://doi.org/10.1016/j.limno.2016.03.005

An, Z., Colman, S.M., Zhou, W., Li, X., Brown, E.T., Jull, A.J.T., Liu, W., Jin, Z., Liu, X., Cheng, P., Liu, Y., Ai, L., Li, X., Liu, X., Xu, X., 2012. Interplay between the Westerlies and Asian monsoon recorded in Lake Qinghai sediments since 32 ka. Sci. Rep. 2, 1–7. https://doi.org/10.1038/srep00619

Appleby, P.G., Oldfield, F., 1978. The calculation of lead-210 dates assuming a constant rate of supply of unsupported 210Pb to the sediment. Catena 5, 1–8.

Avouac, J., Dobrernez, J., Bourjot, L., 1996. Palaeoclimatic interpretation of a topographic profile across middle Holocene regressive shorelines of Longmu Co. Palaeogeogr. Palaeoclimatol. Palaeoecol. 120, 93–104.

Bird, B.W., Polisar, P.J., Lei, Y., Thompson, L.G., Yao, T., Finney, B.P., Bain, D.J., Pompeani, D.P., Steinman, B.A., 2014. A Tibetan lake sediment record of Holocene Indian summer monsoon variability. Earth Planet. Sci. Lett. 399, 92–102. https://doi.org/10.1016/j.epsl.2014.05.017

Blaauw, M., Christen, A.J., 2011. Flexible Paleoclimate Age-Depth Models Using an Autoregressive Gamma Process. Bayesian Anal. 6, 457–474. https://doi.org/10.1214/11-BA618

Chen, F., Jia, J., Chen, J., Li, G., Zhang, X., Xie, H., Xia, D., Huang, W., An, C., 2016. A persistent

Holocene wetting trend in arid central Asia, with wettest conditions in the late Holocene, revealed by multi-proxy analyses of loess-paleosol sequences in Xinjiang, China. Quat. Sci. Rev. 146, 134–146. https://doi.org/10.1016/j.quascirev.2016.06.002

Chen, Y., Zong, Y., Li, B., Li, S., Aitchison, J.C., 2013. Shrinking lakes in Tibet linked to the weakening Asian monsoon in the past 8.2ka. Quat. Res. (United States) 80, 189–198. https://doi.org/10.1016/j.yqres.2013.06.008

Christen, J.A., Pérez, E.S., 2010. A new robust statistical model for radiocarbon data, Radiocarbon 51, 1047–1059.

Clement, A.C., 1999. Orbital controls on ENSO and the tropical climate. Paleoceanography 14, 441–456.

Clement, A.C., Seager, R., Cane, M.A., Zebiak, S., 1996. An ocean dynamical thermostat. J. Clim. 9, 2190–2196.

Conroy, J.L., Hudson, A.M., Overpeck, J.T., Liu, K., Wang, L., Cole, J.E., 2017. The primacy of multidecadal to centennial variability over late-Holocene forced change of the Asian Monsoon on the southern Tibetan Plateau. Earth Planet. Sci. Lett. 458, 337 – 348.

Craig, H., 1965. The measurement of oxygen isotope palaeotempera- tures. In: Tongiorgi, E. (Ed.), Stable Isotopes in Oceanographic Studies and Palaeotemperatures. Pisa, Consiglio Nazionale delle Ricerche

Laboratorio di Geologia Nucleare, pp. 161–182.

Deng, S., Dong, H., Lv, G., Jiang, H., Yu, B., Bishop, M. E., 2010. Microbial dolomite precipitation using sulfate reducing and halophilic bacteria: Results from Qinghai Lake, Tibetan Plateau, NW China. Chem. Geol. 278, 151–159.

Fan, H., Gasse, F., Huc, A., Li, Y., Sifeddine, A., Soulie-Marsche, I., 1996. Holocene environmental changes in Bangong Co basin (Western Tibet). Part 3: Biogenic remains. Palaeogeogr. Palaeoclimatol. Palaeoecol. 120, 65–78.

Fleitmann, D., Burns, S.J., Mangini, A., Mudelsee, M., Kramers, J., Villa, I., Neff, U., Al-Subbary, A.A., Buettner, A., Hippler, D., Matter, A., 2007. Holocene ITCZ and Indian monsoon dynamics recorded in stalagmites from Oman and Yemen (Socotra). Quat. Sci. Rev. 26, 170–188. https://doi.org/10.1016/j.quascirev.2006.04.012

Fleitmann, D., Burns, S.J., Mudelsee, M., Neff, U., Kramers, J., Mangini, A., Matter, A., 2003. Holocene Forcing of the Indian Monsoon Recorded in a Stalagmite from Southern Oman. Science 1737, 1737–1739. https://doi.org/10.1111/j.1461-0248.2008.01280.x

Folk, R.L., Land, L.S., 1975. Mg/Ca Ratio and Salinity: Two controls over crystallization of dolomite. Amer. Assoc. Petrol. Geol. Bull. 59, 60–68.

Gaines, A.M., 1980. Dolomitization kinetics: recent experimental studies. Soc. Econ. Paleontol. Mineral. Spec. 28, 81–86.

Garrison, R.E., Graham, S.A., 1984. Early diagenetic dolomites and the origin of dolomite-bearing breccias, lower Monterey formation, Arroyo Seco, Monterey County, California. In: Garrison, R.E., Kastner, M., Zenger, D.H (Eds.), Dolomites of the Monterey Formation and Other Organic-Rich Units. Spec. Publ.-SEPM (Pacific Section, Los Angeles) vol. 41, pp. 87–101.

Gasse, F., Arnold, M., Fonres, J.C., Fort, M., Gibert, E., Huc, A., Li, B., Li, Y., Liu, Q., Melleres, F., Van Campo, E., Wang, F., Zhang, Q., 1991. A 13,000-year climate record from western Tibet. Nature 353, 742–745.

Gasse, F., Fontes, J.C., Van Campo, E., Wei, K., 1996. Holocene environmental changes in Bangong Co basin (Western Tibet). Part 4: Discussion and conclusions. Palaeogeogr. Palaeoclimatol. Palaeoecol. 120, 79–92. https://doi.org/10.1016/0031-0182(95)00035-6

Griffiths, H.I., Holmes, J.A., 2000. Non-marine ostracods & Quaternary palaeoenvironments. Technical Guide 8. Quaternary Research Association, London.

Grossman, E.L., Ku, T.L., 1986. Oxygen and carbon isotope fractionation in biogenic Aragonite: temperature effects. Chem. Geol. 59, 59–74.

Guo, X., Tian, L., Wen, R., Yu, W., Qu, D., 2017. Controls of precipitation $\delta^{18}O$ on the northwestern Tibetan Plateau: A case study at Ngari station. Atmos. Res. 189, 141–151. https://doi.org/10.1016/j.atmosres.2017.02.004

Håkanson, L., Jansson, M., 1983. Principles of lake sedimentology. Springer-Verlag, Berlin, Heidelberg, New York, Tokyo.

Henderson, A.C.G., Holmes, J.A., Leng, M.J., 2010. Late Holocene isotope hydrology of Lake Qinghai, NE Tibetan Plateau: Effective moisture variability and atmospheric circulation changes. Quat. Sci. Rev. 29, 2215–2223. https://doi.org/10.1016/j.quascirev.2010.05.019

Heiri, O., Lotter, A.F., Lemcke, G., 2001. Loss on ignition as a method for estimating organic and carbonate content in sediments: reproducibility and comparability of results. J. paleolimnol. 25, 101 - 110

Hou, J., D’Andrea, W.J., Liu, Z., 2012. The influence of ^{14}C reservoir age on interpretation of paleolimnological records from the Tibetan Plateau. Quat. Sci. Rev. 48, 67–79.

Hou, J., D’Andrea, W.J., Wang, M., He, Y., Liang, J., 2017. Influence of the Indian monsoon and the subtropical jet on climate change on the Tibetan Plateau since the late Pleistocene. Quat. Sci. Rev. 163, 84–94. https://doi.org/10.1016/j.quascirev.2017.03.013

Hou, J., Huang, Y., Zhao, J., Liu, Z., Colman, S., An, Z., 2016. Large Holocene summer temperature oscillations and impact on the peopling of the northeastern Tibetan Plateau. Geophys. Res. Lett. 43, 1323–1330. https://doi.org/10.1002/2015GL067317

Huang, X., Sillanpää, M., Duo, B., Gjessing, E.T., 2008. Water quality in the Tibetan Plateau: Metal contents of four selected rivers. Environ. Pollut. 156, 270–277. https://doi.org/10.1016/j.envpol.2008.02.014

Hudson, A.M., Quade, J., Huth, T.E., Lei, G., Cheng, H., Edwards, L.R., Olsen, J.W., Zhang, H., 2015. Lake level reconstruction for 12.8-2.3ka of the Ngangla Ring Tso closed-basin lake system, southwest Tibetan Plateau. Quat. Res. (United States) 83, 66–79. https://doi.org/10.1016/j.yqres.2014.07.012

Huth, T., Hudson, A.M., Quade, J., Guoliang, L., Hucai, Z., 2015. Constraints on paleoclimate from 11.5 to 5.0 ka from shoreline dating and hydrologic budget modeling of Baqan Tso, southwestern Tibetan Plateau. Quat. Res. (United States) 83, 80–93. https://doi.org/10.1016/j.yqres.2014.07.011

Kong, P., Na, C., Brown, R., Fabel, D., Freeman, S., Xiao, W., Wang, Y., 2011. Cosmogenic ^{10}Be and ^{26}Al dating of paleolake shorelines in Tibet. J. Asian Earth Sci. 41: 263–273

Leng, M.J., Marshall, J.D., 2004. Palaeoclimate interpretation of stable isotope data from lake sediment archives. Quat. Sci. Rev. 23, 811–831. https://doi.org/10.1016/j.quascirev.2003.06.012

Li, J., Dodson, J., Yan, H., Cheng, B., Zhang, X., Xu, Q., Ni, J., Lu, F., 2017b. Quantitative precipitation estimates for the northeastern Qinghai-Tibetan Plateau over the last 18,000 years. J. Geophys. Res. 122, 5132–5143. https://doi.org/10.1002/2016JD026333

Li, X., Wang, M., Zhang, Y., Lei, L., Hou, J., 2017a. Holocene climatic and environmental change on the western Tibetan Plateau revealed by glycerol dialkyl glycerol tetraethers and leaf wax deuterium-to-hydrogen ratios at Aweng Co. Quat. Res. 87, 455–467. https://doi.org/10.1017/qua.2017.9

Liu, W., Feng, X., Ning, Y., Zhang, Q., Cao, Y., An, Z., 2005. $\delta^{13}C$ variation of C_3 and C_4 plants across an Asian monsoon rainfall gradient in arid northwestern China. Glob. Chang. Biol. 11, 1094–1100. https://doi.org/10.1111/j.1365-2486.2005.00969.x

Liu, X., Lai, Z., Zeng, F., Madsen, D.B., Chong-Yi, E., 2013. Holocene lake level variations on the Qinghai-Tibetan Plateau, Int. J. Earth Sci. 102, 2007–2016

Liu, X., Madsen, D.B., Liu, R., Sun, Y., Wang, Y., 2016. Holocene lake level variations of Longmu Co, western Qinghai-Tibetan Plateau. Environ. Earth Sci. 75, 1–14. https://doi.org/10.1007/s12665-015-5188-7

Meisch, C., 2000. Freshwater Ostracoda of Western and Central Europe. Spektrum Akademischer Verlag

Heidelberg, Berlin.

Meyers, P.A., Ishiwatari, R., 1993. Lacustrine organic geochemistry-an overview of indicators of organic matter sources and diagenesis in lake sediments. Org. Geochem. 20, 867–900. https://doi.org/10.1016/0146-6380(93)90100-P

Meyers, P.A., Teranes, J.L., 2001. Sediment organic matter, in: Last, W.M., Smol, J.P. (Eds.), Tracking environmental changes using lake sediments. Volume 2: physical and geochemical methods. Kluwer Academic Publishers, Dordrecht, The Netherlands, pp. 247.

Mischke, S., Aichner, B., Diekmann, B., Herzschuh, U., Plessen, B., Wünnemann, B., Zhang, C., 2010. Ostracods and stable isotopes of a late glacial and Holocene lake record from the NE Tibetan Plateau. Chem. Geol. 276, 95–103. https://doi.org/10.1016/j.chemgeo.2010.06.003

Mischke, S., Herzschuh, U., Kurschner,H., Fuchs, D., Zhang, J., Meng, F., Sun, Z., 2003. Sub-Recent Ostracoda from Qilian Mountains (NW China) and their ecological significance. Limonologica 292, 280–292. https://doi.org/10.1016/S0075-9511(03)80023-3

Mischke, S., Herzschuh, U., Massmann, G., Zhang, C., 2007. An ostracod-conductivity transfer function for Tibetan lakes. J. Paleolimnol. 38, 509–524. https://doi.org/10.1007/s10933-006-9087-5

Mischke, S., Lai, Z., Zhang, C., 2014. Re-assessment of the paleoclimate implications of the Shell Bar in the Qaidam Basin, China. J. Paleolimnol. 51, 179–195. https://doi.org/10.1007/s10933-012-9674-6 https://doi.org/10.1016/j.palaeo.2008.06.002

Mishra, P.K., Prasad, S., Anoop, A., Plessen, B., Jehangir, A., Gaye, B., Menzel, P., Weise, S.M., Yousuf, A.R., 2015. Carbonate isotopes from high altitude Tso Moriri Lake (NW Himalayas) provide clues to late glacial and Holocene moisture source and atmospheric circulation changes. Palaeogeogr. Palaeoclimatol. Palaeoecol. 425, 76–83. https://doi.org/10.1016/j.palaeo.2015.02.031

Müller, G., Irion, G., Förstner, U., 1972. Formation and diagenesis of inorganic Ca-Mg carbonates in the lacustrine environment. Naturwissenschften 59, 158–164.

Opitz, S., Wünnemann, B., Aichner, B., Dietze, E., Hartmann, K., Herzschuh, U., IJmker, J., Lehmkuhl, F., Li, S., Mischke, S., Plotzki, A., Stauch, G., Diekmann, B., 2012. Late Glacial and Holocene development of Lake Donggi Cona, north-eastern Tibetan Plateau, inferred from sedimentological analysis. Palaeogeogr. Palaeoclimatol. Palaeoecol. 337–338, 159–176. https://doi.org/10.1016/j.palaeo.2012.04.013

Peng, Y., Xiao, J., Nakamura, T., Liu, B., Inouchi, Y., 2005. Holocene East Asian monsoonal precipitation pattern revealed by grain-size distribution of core sediments of Daihai Lake in Inner Mongolia of north-central China. Earth Planet. Sci. Lett. 233, 467–479.

Qiang, M., Song, L., Jin, Y., Li, Y., Liu, L., Zhang, J., Zhao, Y., Chen, F., 2017. A 16-ka oxygen-isotope record from Genggahai Lake on the northeastern Qinghai-Tibetan Plateau: Hydroclimatic evolution and changes in atmospheric circulation. Quat. Sci. Rev. 162, 72–87. https://doi.org/10.1016/j.quascirev.2017.03.004

Rades, E.F., Hetzel, R., Xu, Q., Ding, L., 2013. Constraining Holocene lake-level highstands on the Tibetan Plateau by ^{10}Be exposure dating: A case study at Tangra Yumco, southern Tibet. Quat. Sci. Rev. 82: 68–77.

Rades, E.F., Tsukamoto, S., Frechen, M., Xu, Q., Ding, L., 2015. A lake-level chronology based on feldspar luminescence dating of beach ridges at the Tangra Yum Co (southern Tibet). Quat. Res. 83: 469–478.

Reimer, P.J., Bard, E., Bayliss, A., Beck, J.W., Blackwell, P.G., Ramsey, C.B., Buck, C.E., Cheng, H., Edwards, R.L., Friedrich, M., Grootes, P.M., Guilderson, T.P., Haflidason, H., Hajdas, I., Hatte, C., Heaton, T.J., Hoffmann, D.L., Hogg, A.G., Hughen, K.A., Kaiser, K.F., Kromer, B., Manning, S.W., Niu, M., Reimer, R.W., Richards, D.A., Scott, E.M., Southon, J.R., Staff, R.A., Turney, C.S.M., van der Plicht, J., 2013. Intcal13 and Marine13 radiocarbon age calibration curves 0 – 50,000 years Cal BP. Radiocarbon 55, 1869–1887. https://doi.org/10.2458/azu_js_rc.55.16947

Roehl, P.O., Weinbrandt, R.M., 1985. West Cat Canyon Field, In: Roehl, P.O., Choquette, P.W. (Eds.), Carbonate Petroleum Reservoirs. Springer, New York, pp. 525–545.

Song, C., Bo, H., Richards, K., Ke, L., Phan, V.H., 2014. Accelerated lake expansion on the Tibetan Plateau in the 2000s: Induced by glacial melting or other processes? Water Resour. Res. 50, 3170–3186. https://doi.org/10.1002/2013WR014724

Steinman, B.A., Rosenmeier, M.F., Abbott, M.B., 2010. The isotopic and hydrologic response of small, closed-basin lakes to climate forcing from predictive models: Simulations of stochastic and mean-state precipitation variations. Limnol. Oceanogr. 55(6), 2246–2261.

Steinman, B.A., Rosenmeier, M.F., Abbott, M.B., Bain, D.J., 2010. The isotopic and hydrologic response of small, closed-basin lakes to climate forcing from predictive models: Application to paleoclimate studies in the upper Columbia River basin. Limnol. Oceanogr. 55(6), 2231–2245.

Stuiver, M., Braziunas, T.F., 1998. Anthropogenic and solar components of hemispheric ^{14}C. Geophys. Res. Lett. 25, 329–332

Sun, H., Qin, J., Wu, Y., 2008. Freeze-thaw cycles and their impacts on ecological process: A review. Soils 40, 505–509 (in Chinese with English abstract).

Sun, Q., Zhou, J., Xiao, J., 2001. Grain-size characteristics of Lake Daihai sediments and its paleo-environment significance. Mar. Geol. Quat. Geol. 21, 93–95 (in Chinese with English abstract).

Tan, L., Cai, Y., Cheng, H., Edwards, L.R., Lan, J., Zhang, H., Li, D., Ma, L., Zhao, P., Gao, Y., 2018. High resolution monsoon precipitation changes on southeastern Tibetan Plateau over the past 2300 years. Quat. Sci. Rev. 195, 122–132.

Tian, L., Yao, T., MacClune, K., White, J.W.C., Schilla, A., Vaughn, B., Vachon, R., Ichiyanagi, K., 2007. Stable isotopic variations in west China: A consideration of moisture sources. J. Geophys. Res. Atmos. 112, 1–12. https://doi.org/10.1029/2006JD007718

Van Campo, E., Cour, P., Hang, S., 1996. Holocene environmental changes in Bangong Co basin (Western Tibet). Part 2: The pollen record. Palaeogeogr. Palaeoclimatol. Palaeoecol. 120, 49–63.

Vasconcelos, C., McKenzie, J. A., Bernasconi, S., Grujic, D., Tiens, A. J., 1995. Microbial mediation as a possible mechanism for natural dolomite formation at low temperatures. Nature, 377, 220–222.

Wang, J., Deng, W., Zhang, P., Zhang, J., 2014. The differences in organic carbon isotope of different size components in lake sediments and its impact on experimental results. J. Lake Sci. 26, 625–631 (in Chinese with English abstract).

Wang, S., Dou, H., 1998. Records of lakes in China (in Chinese). Science Press, Beijing.

Wang, W., Feng, Z., 2013. Holocene moisture evolution across the Mongolian Plateau and its surrounding areas: A synthesis of climatic records. Earth Sci. Rev. 122, 38–57.

https://doi.org/10.1016/j.earscirev.2013.03.005

Wang, K., Jiang, H., Zhao, H., 2005. Atmospheric vapor transport from westerly and monsoon over the Northwest China. Adv. Water Sci. 16, 432–438 (in Chinese with English abstract)

Wünnemann, B., Yan, D., Ci, R., 2015. Morphodynamics and lake level variations at Paiku Co, southern Tibetan Plateau, China. Geomorphology 246, 489–501. https://doi.org/10.1016/j.geomorph.2015.07.007

Xie, M., Zhu, L., Peng, P., Wang, J., Wang, Y., Schwalb, A., 2009. Ostracod assemblages and their environmental significance from the lake core of the Nam Co on the Tibetan Plateau 8.4 ka BP. J. Geogr. Sci. 19, 387–402. https://doi.org/10.1007/s11442-009-0387-3

Yao, T., Masson-delmotte, V., Gao, J., Yu, W., Yang, X., Risi, C., Sturm, C., Werner, M., Zhao, H., He, Y., Ren, W., 2013. A Review of Climatic Controls on δ18O in Precipitation Over the Tibetan Plateau: Observations and Simulations. Rev. Geophys. 51, 525–548. https://doi.org/10.1002/rog.20023

Zhang, J., Chen, F., Holmes, J.A., Li, H., Guo, X., Wang, J., Li, S., Lü, Y., Zhao, Y., Qiang, M., 2011. Holocene monsoon climate documented by oxygen and carbon isotopes from lake sediments and peat bogs in China: a review and synthesis. Quat. Sci. Rev. 30, 1973–1987. https://doi.org/10.1016/j.quascirev.2011.04.023

Zhang, Y., Jones, M., Zhang, J., McGowan, S., Metcalfe, S., 2020. Can $\delta^{18}O$ help indicate the causes of recent lake area expansion on the western Tibetan 1 Plateau? A case study from Aweng Co. J. Paleolimnol. https://doi.org/10.1007/s10933-020-00158-6

Zhang, J., Ma, X., Qiang, M., Huang, X., Li, S., Guo, X., Henderson, A.C.G., Holmes, J.A., Chen, F., 2016a. Developing inorganic carbon-based radiocarbon chronologies for Holocene lake sediments in arid NW China. Quat. Sci. Rev. 144, 66–82. https://doi.org/10.1016/j.quascirev.2016.05.034

Zhang, C., Zhang, W., Zhang, L., Xiaoyu, W., Imbabazi, B., 2016b. The Characteristics of Carbon and Oxygen Isotopes of Carbonates and Carbon Isotopes of Organic Matter of Bulk Sediments and Their Responses to Lake Environments in Western and Northeastern China. Bull. Mineral. Petrol. Geochemistry 35, 609–617 (in Chinese with English abstract).

Zhao, C., Liu, Z., Rohling, E.J., Yu, Z., Liu, W., He, Y., Zhao, Y., Chen, F., 2013. Holocene temperature fluctuations in the northern Tibetan Plateau. Quat. Res. (United States) 80, 55–65. https://doi.org/10.1016/j.yqres.2013.05.001

Zhou, X., Zhu, L., Yang, W., Jiang, L., 2011. Features of hydrocarbon source rocks of Paleogene Niubao Group in Awengcuo basin, Tibet Plateau, China. J. Chengdu Univ. Technol (Science Technol. Ed.) 38, 199–203 (in Chinese with English abstract).

Appendices

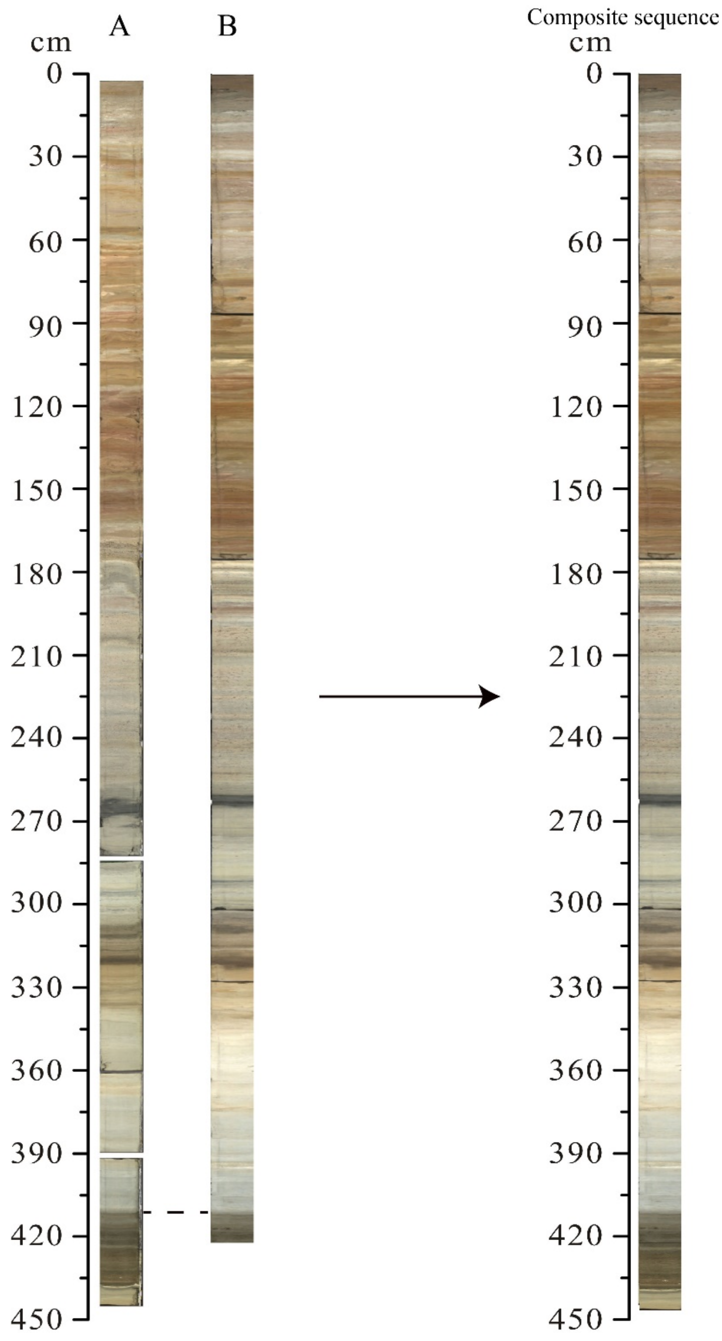

Fig. A.1. The sediment cores of AWC2015A, AWC2015B and the composite sequence. The position of the dashed line is 411.5 cm.

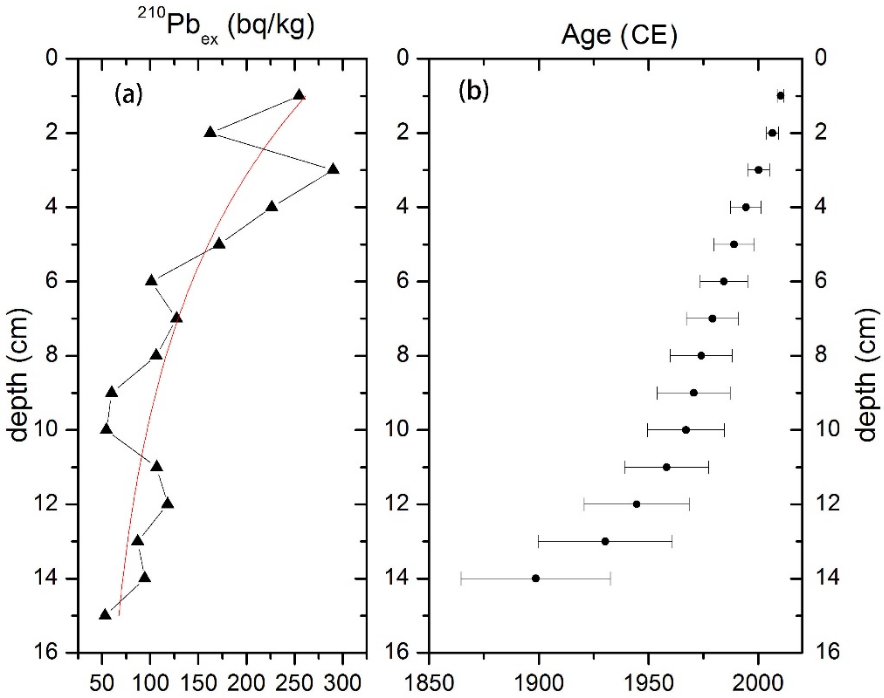

Fig. A.2. The results of ^{210}Pb dating. (a) is the depth profile of $^{210}Pb_{ex}$. (b) is the age-depth model developed using the CRS method, with errors bars.

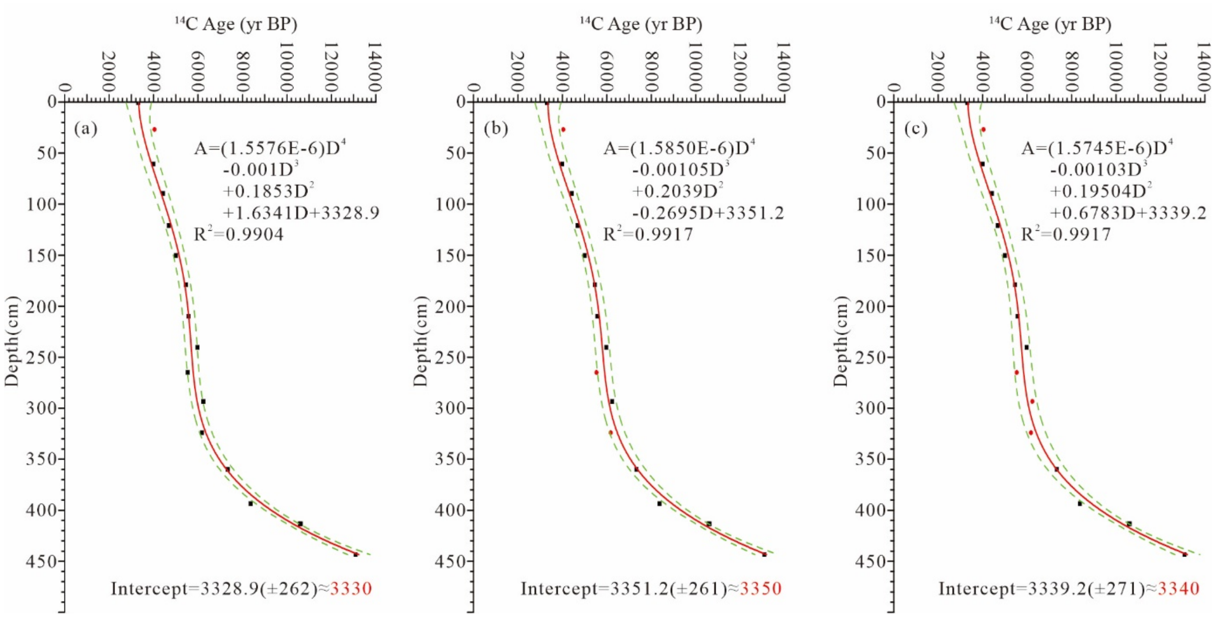

Fig. A. 3: Calculation of the reservoir effect (RE) under different scenarios with inclusion/exclusion of the dating point at 293.5 cm. The red line is the regression line and green lines are the confidence lines at 95 % level. Red dots are excluded in the regressions. (a) only one reversed age at 26.9 cm is excluded; (b) three reversed ages are excluded, which is used in this paper; (c) four ages are excluded.

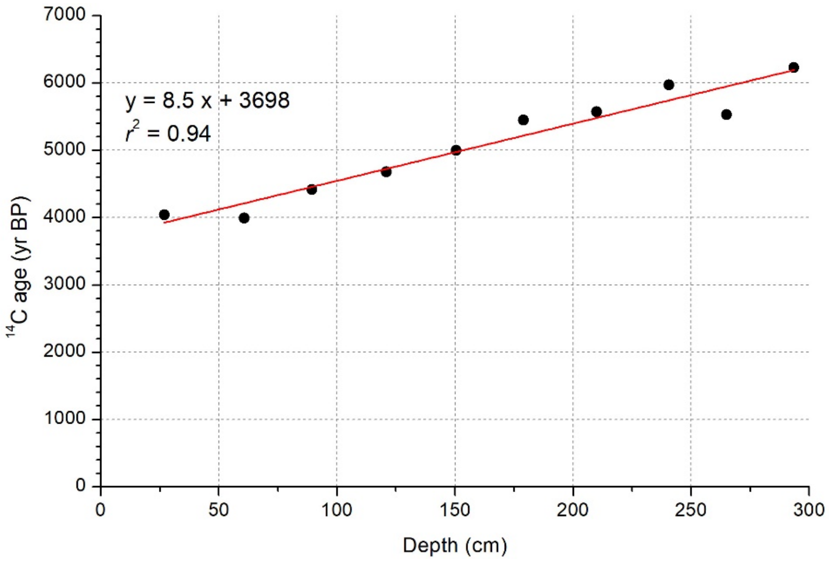

Fig. A. 4. Linear regression of ^{14}C dates for the upper 300 cm of core AWC2015 (the ^{14}C date at 0.5 cm is excluded).

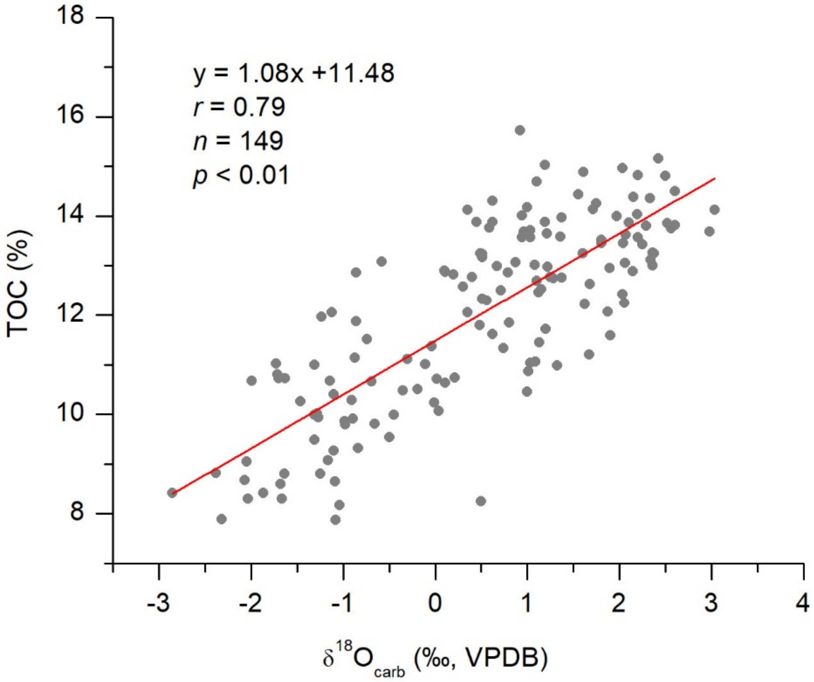

Fig. A. 5. Correlation of $\delta^{18}O_{carb}$ and TOC in the core AWC2015 during the past 3.1 kyr.

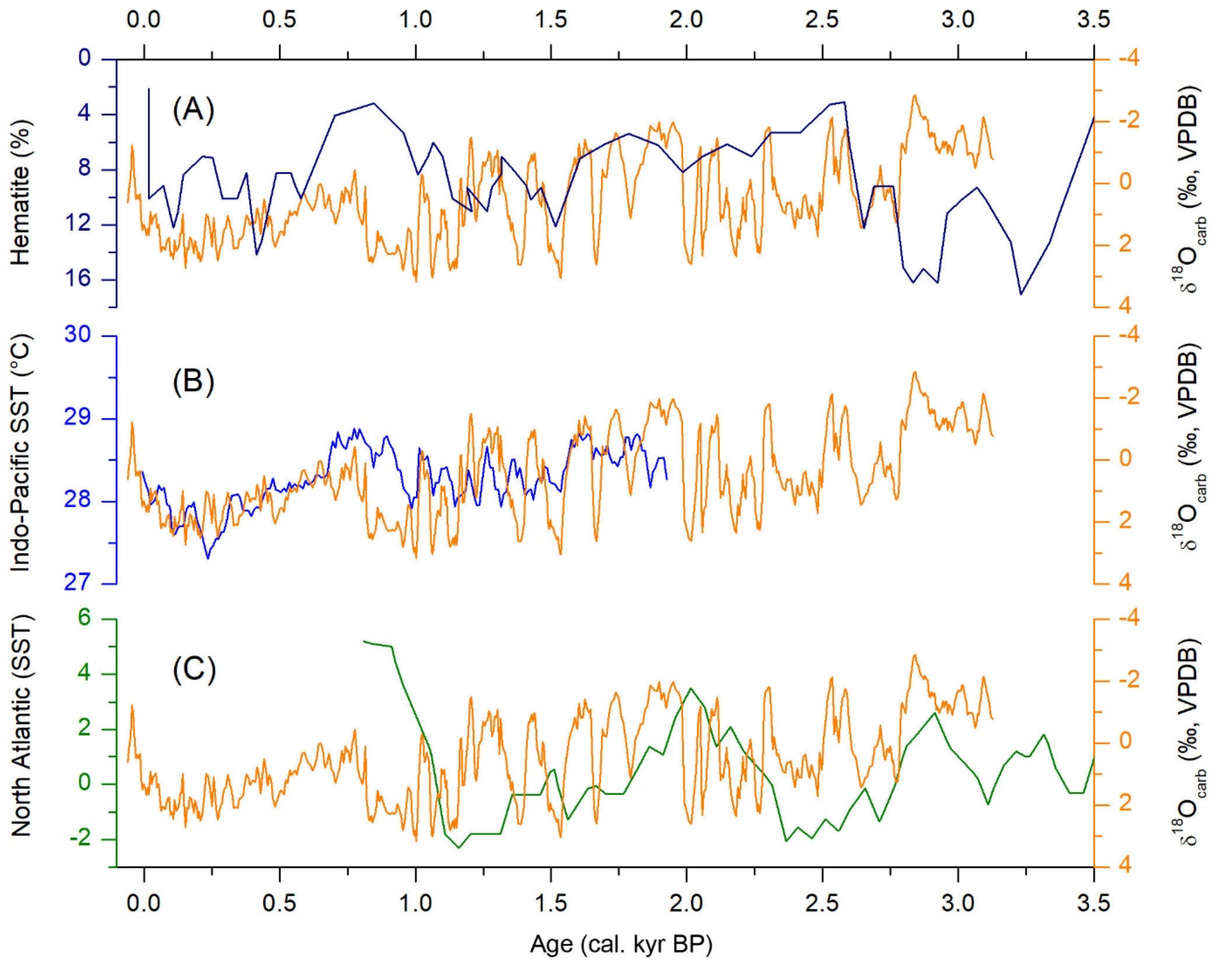

Fig. A. 6: Comparisons of the late Holocene $\delta^{18}O_{carb}$ (orange lines) with the possible driving factors. (A): The hematite-stained grains from the North Atlantic Ocean (dark blue line; Bond et al., 2001). (B): Reconstructed Indo-Pacific sea surface temperature (SST; blue line) (Oppo et al., 2009). (C): Detrended PC 1 of 24 records of North Atlantic SST (Feng et al., 2009).

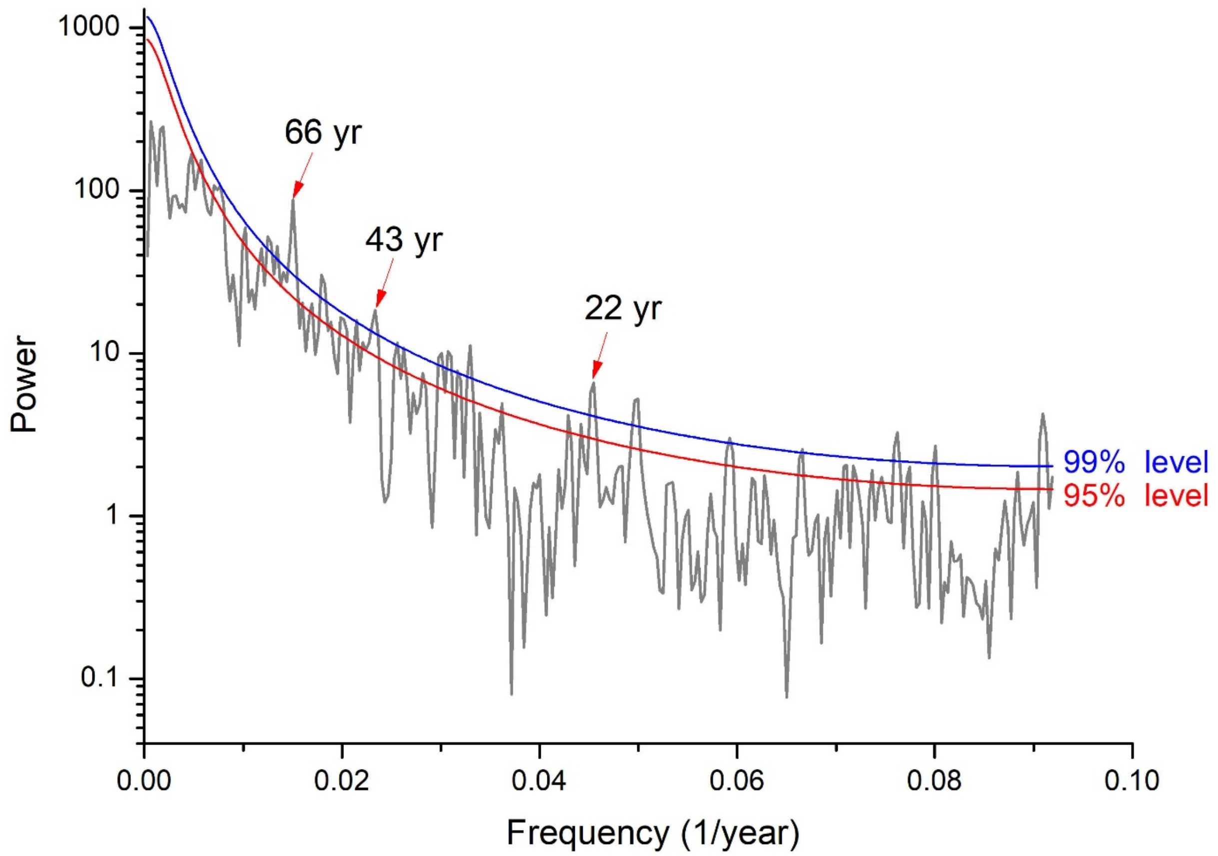

Fig. A. 7. Power spectrum analysis of $\delta^{18}O_{carb}$ record since 3.1 cal. kyr BP from core AWC2015.

References:

Bond, G., Kromer, B., Beer, J., Muscheler, R., Evans, M.N., Showers, W., Hoffman, S., Lotti-Bond, R., Hajdas, I., Bonani, G., Bonani, G., 2001. Persistent Solar Influence on North Atlantic Climate During the Holocene. Science 294, 2130–2136.

Feng, S., Hu, Q., Oglesby, R.J., 2009. AMO-like variations of Holocene sea surface temperature in the North Atlantic Ocean. Clim. Past Discuss. 2009, 2465 – 2496.

Oppo, DW., Rosenthal, Y., Linsley, B.K., 2009. 2000-year-long temperature and hydrology reconstructions from the Indo-Pacific warm pool. Nature 460: 1113 – 1116.

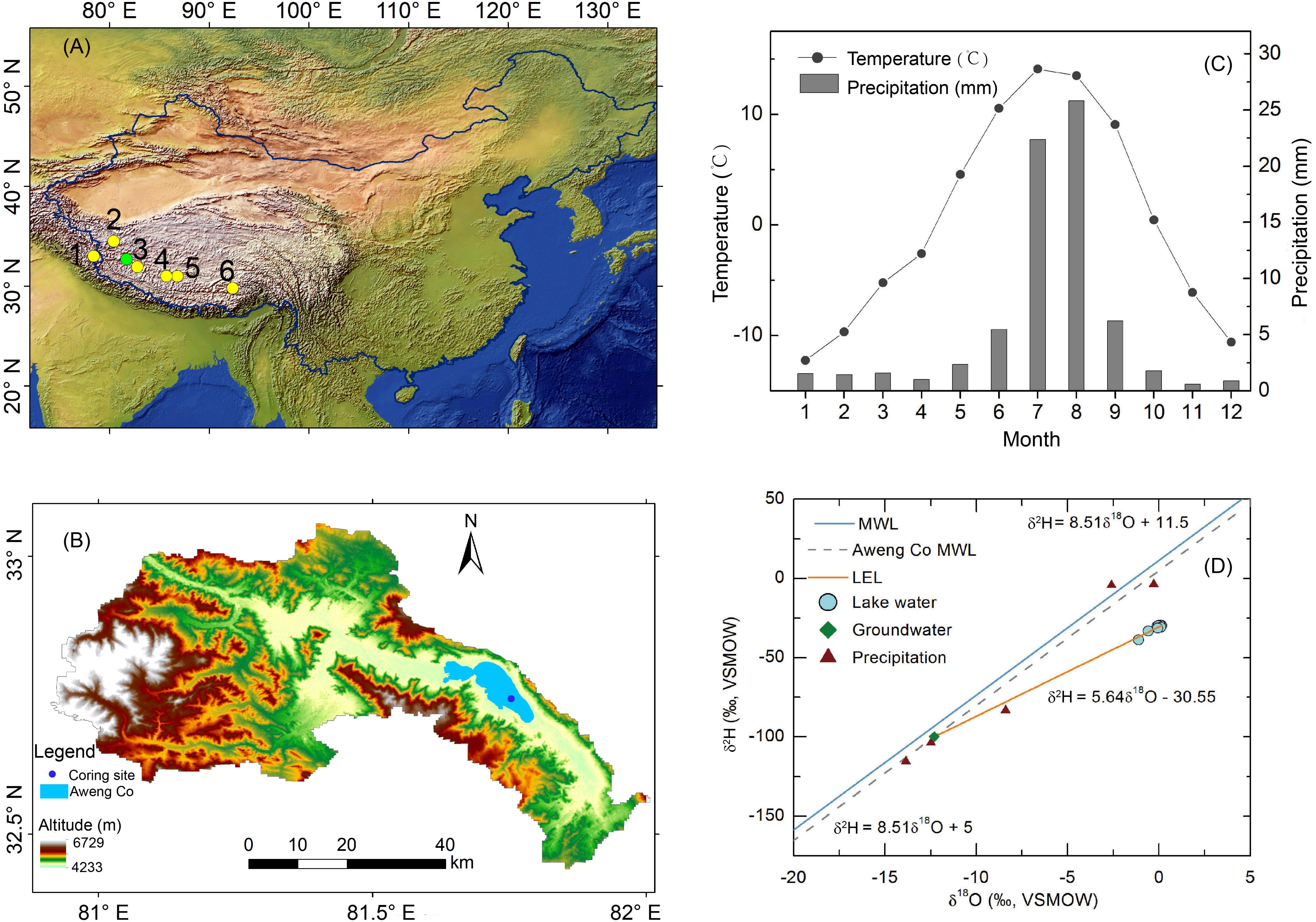

(A)
80° E
90° E
100° E
110° E
120° E
130° E
50° N
40° N
30° N
20° N
1
2
3
4
5
6
(B)
33° N
32.5° N
81° E
81.5° E
82° E
N
Legend
Coring site
Aweng Co
Altitude (m)
6729
4233
0
10
20
40
km
(C)
Temperature (℃)
Precipitation (mm)
Month
(D)
MWL
Aweng Co MWL
LEL
Lake water
Groundwater
Precipitation
$\delta^2H = 8.51\delta^{18}O + 11.5$
$\delta^2H = 5.64\delta^{18}O - 30.55$
$\delta^2H = 8.51\delta^{18}O + 5$
δ^2H (‰, VSMOW)
$\delta^{18}O$ (‰, VSMOW)

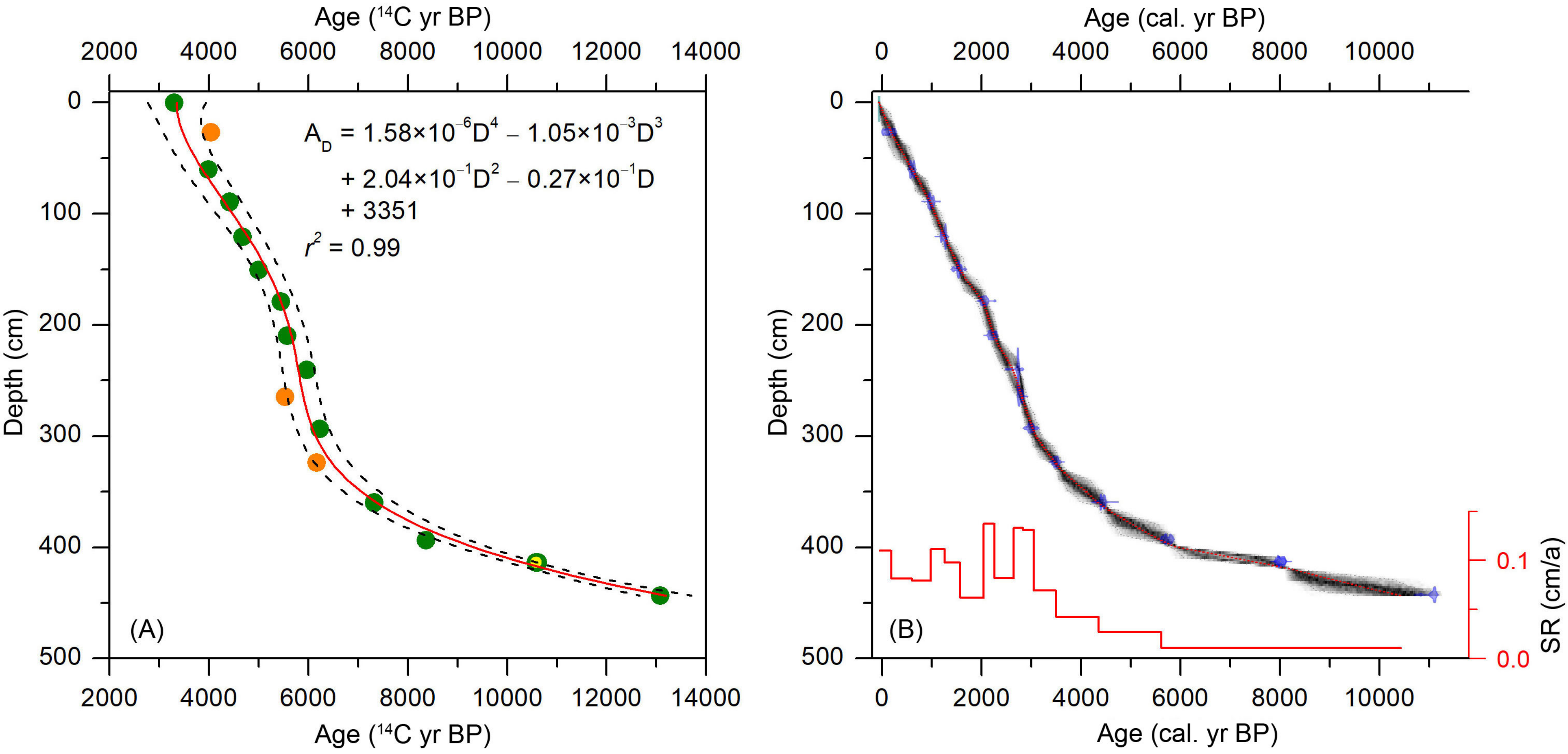

Age (^{14}C yr BP)
2000
4000
6000
8000
10000
12000
14000
Depth (cm)
0
100
200
300
400
500
$A_D = 1.58\times10^{-6}D^4 - 1.05\times10^{-3}D^3 + 2.04\times10^{-1}D^2 - 0.27\times10^{-1}D + 3351$
$r^2 = 0.99$
(A)
Age (cal. yr BP)
0
2000
4000
6000
8000
10000
Depth (cm)
SR (cm/a)
0.1
0.0
(B)

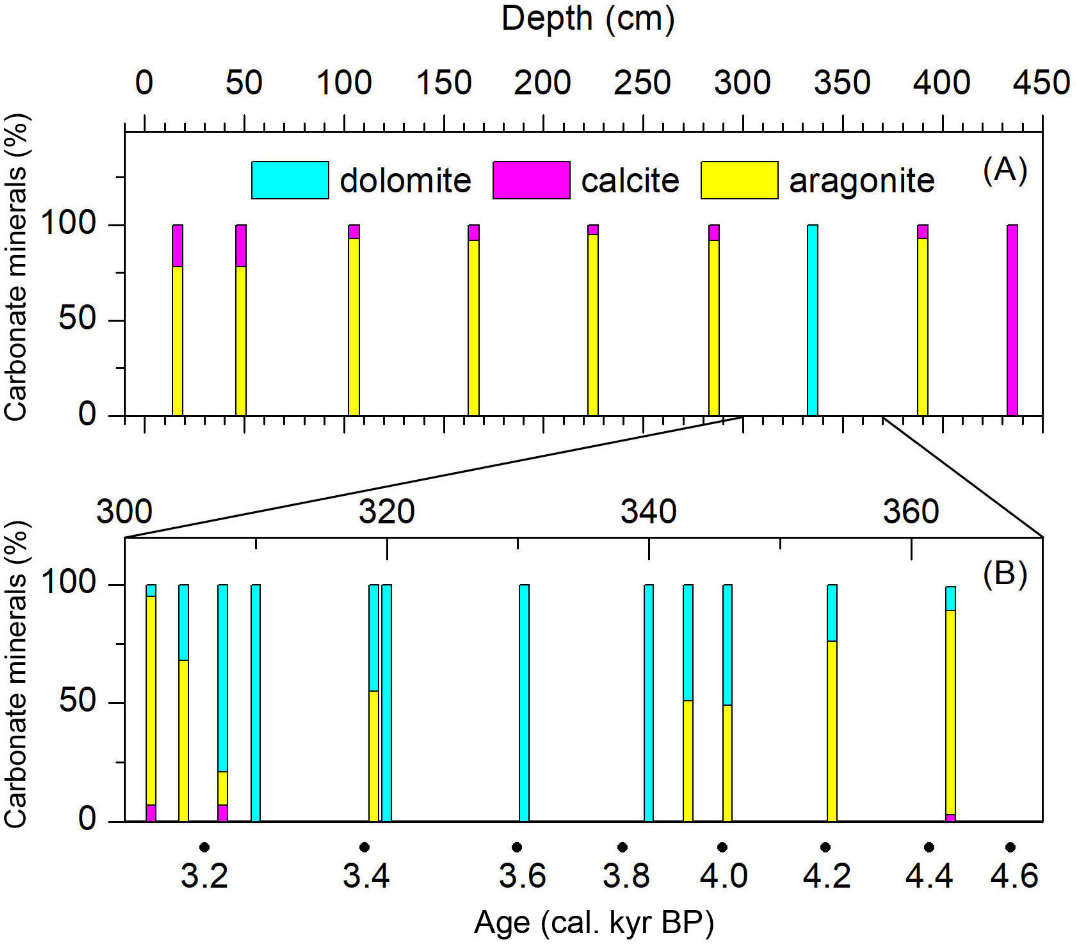

Depth (cm)
0
50
100
150
200
250
300
350
400
450
Carbonate minerals (%)
100
50
0
dolomite
calcite
aragonite
(A)
300
320
340
360
(B)
3.2
3.4
3.6
3.8
4.0
4.2
4.4
4.6
Age (cal. kyr BP)

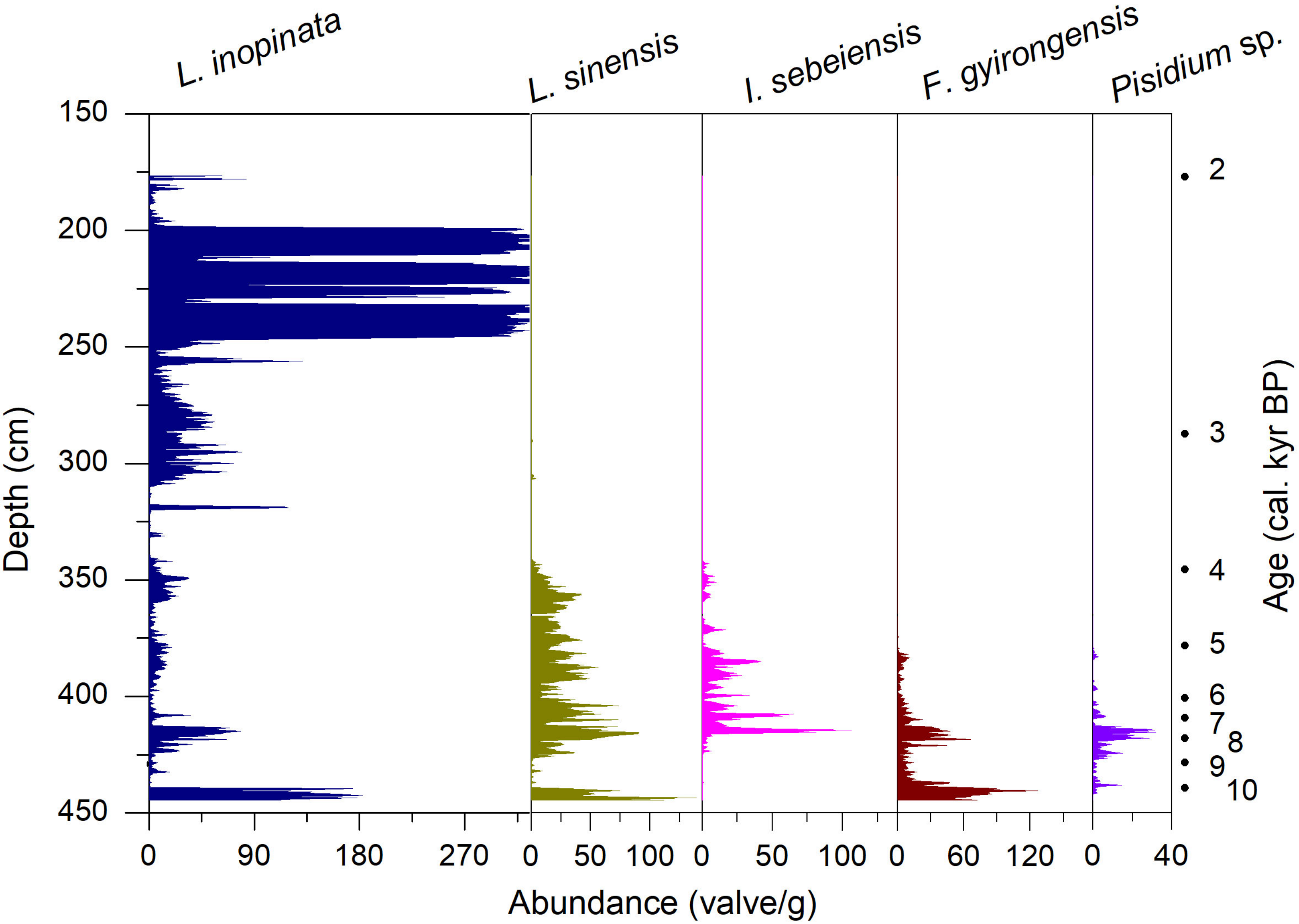
L. inopinata
L. sinensis
I. sebeiensis
F. gyirongensis
Pisidium sp.
Depth (cm)
150
200
250
300
350
400
450
Age (cal. kyr BP)
2
3
4
5
6
7
8
9
10
0
90
180
270
0
50
100
0
50
100
0
60
120
0
40
Abundance (valve/g)

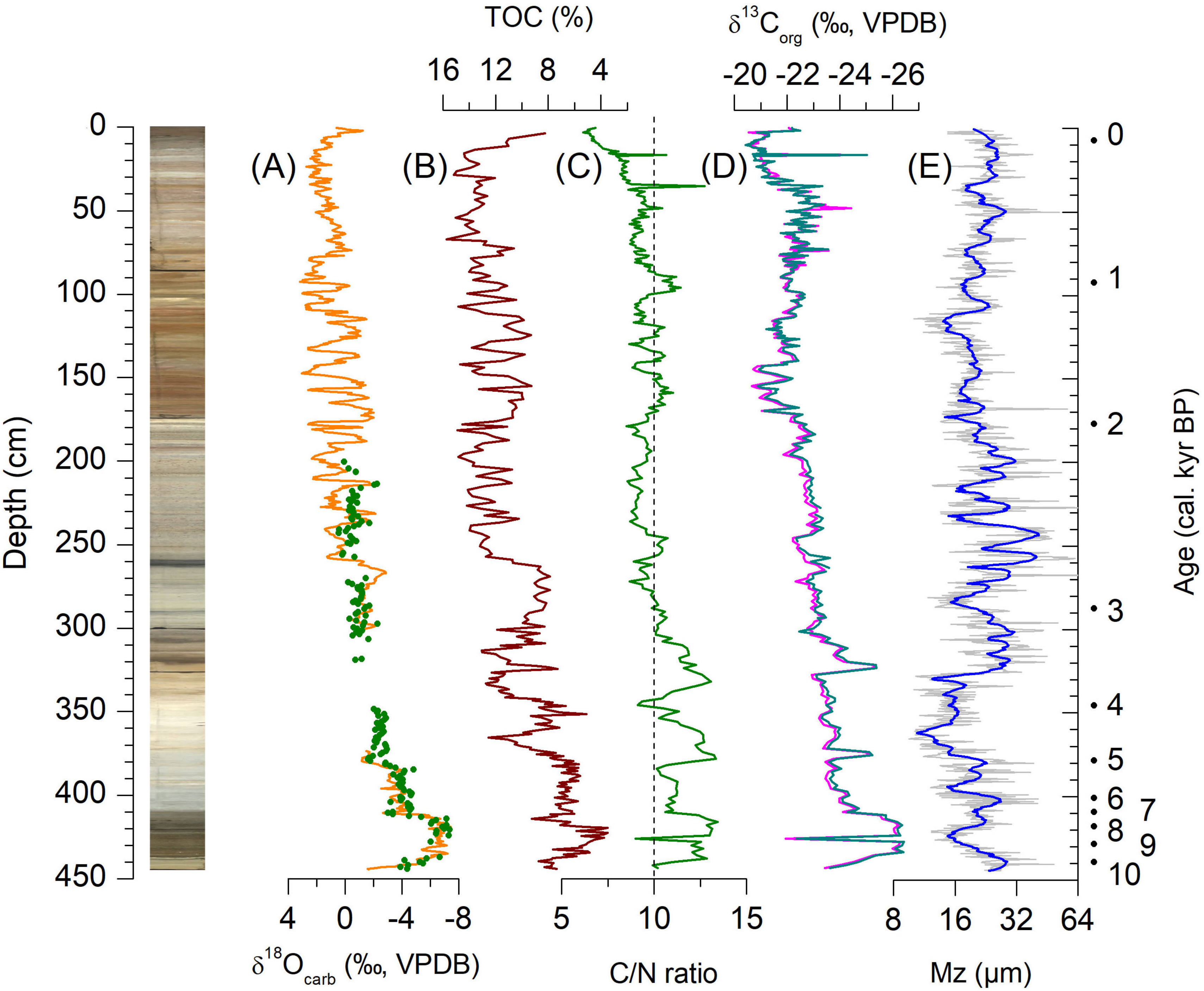

TOC (%)
16 12 8 4
δ13Corg (‰, VPDB)
-20 -22 -24 -26
Depth (cm)
0 50 100 150 200 250 300 350 400 450
(A) (B) (C) (D) (E)
Age (cal. kyr BP)
0 1 2 3 4 5 6 7 8 9 10
4 0 -4 -8
δ18Ocarb (‰, VPDB)
5 10 15
C/N ratio
8 16 32 64
Mz (μm)

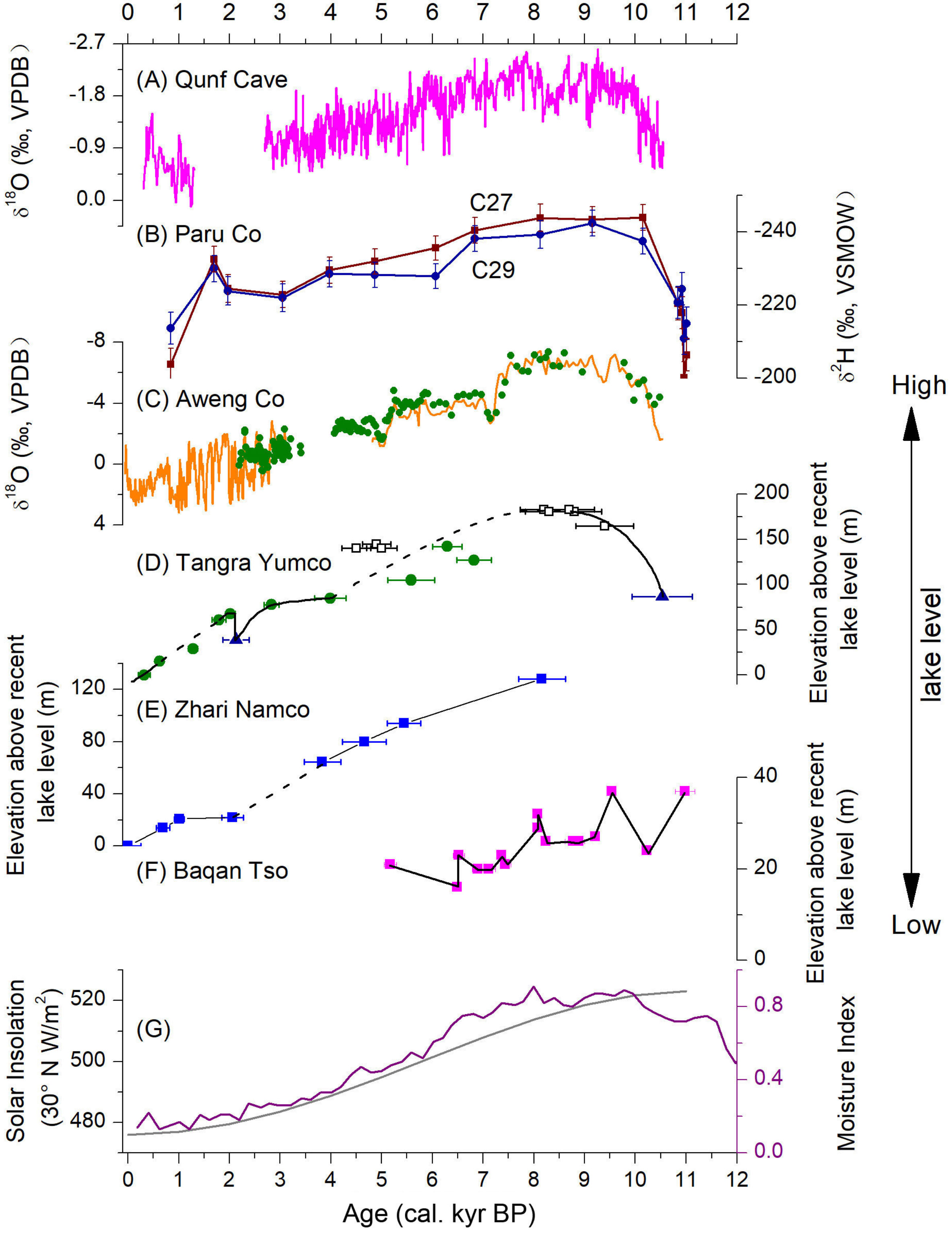

(A) Qunf Cave
δ18O (‰, VPDB)
(B) Paru Co
C27
C29
δ2H (‰, VSMOW)
(C) Aweng Co
δ18O (‰, VPDB)
(D) Tangra Yumco
Elevation above recent lake level (m)
(E) Zhari Namco
Elevation above recent lake level (m)
(F) Baqan Tso
Elevation above recent lake level (m)
(G)
Solar Insolation (30° N W/m2)
Moisture Index
High
lake level
Low
Age (cal. kyr BP)

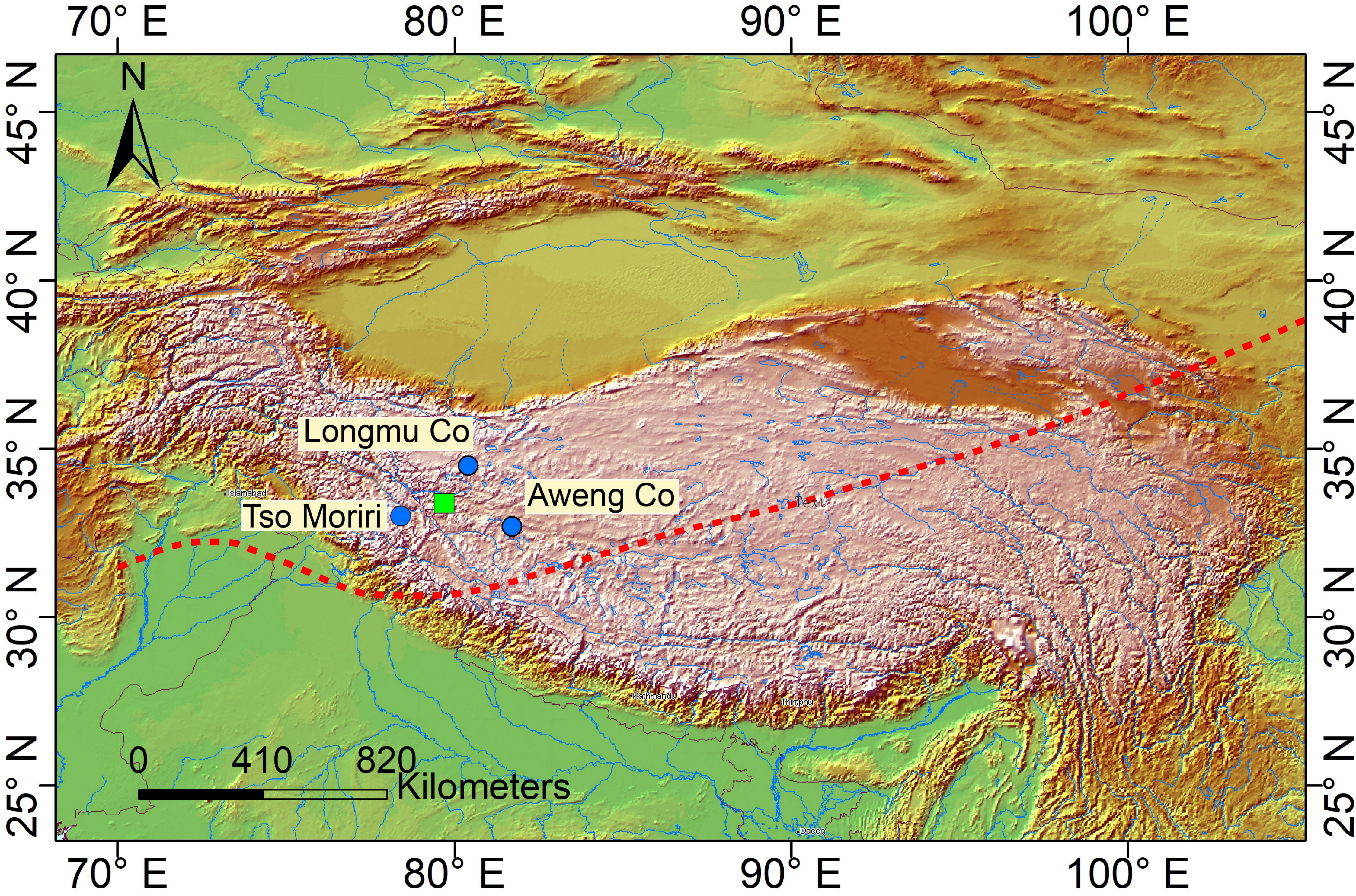

70° E
80° E
90° E
100° E
45° N
40° N
35° N
30° N
25° N
N
Longmu Co
Aweng Co
Tso Moriri
Islamabad
Text
Kathmandu
Thimphu
Dacca
0
410
820
Kilometers

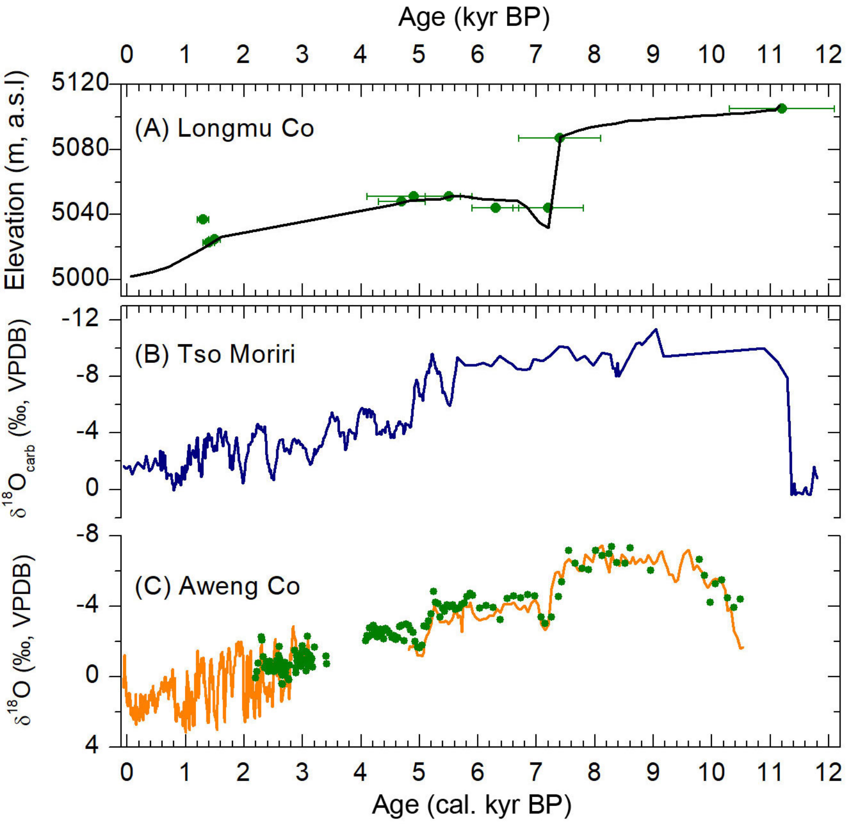

Age (kyr BP)
0 1 2 3 4 5 6 7 8 9 10 11 12
Elevation (m, a.s.l)
5120
5080
5040
5000
(A) Longmu Co
$\delta^{18}O_{carb}$ (‰, VPDB)
-12
-8
-4
0
(B) Tso Moriri
$\delta^{18}O$ (‰, VPDB)
-8
-4
0
4
(C) Aweng Co
0 1 2 3 4 5 6 7 8 9 10 11 12
Age (cal. kyr BP)